

Privacy-Preserving Multiple Tensor Factorization for Synthesizing Large-Scale Location Traces

Takao Murakami
AIST, Tokyo, Japan
takao-murakami at
aist.go.jp

Koki Hamada
NTT, Tokyo, Japan
hamada.koki at
lab.ntt.co.jp

Yusuke Kawamoto
AIST, Tsukuba, Japan
yusuke.kawamoto at
aist.go.jp

Takuma Hatano
NSSOL, Yokohama, Japan
hatano.takuma.hq2 at
jp.nssol.nssmc.com

ABSTRACT

With the widespread use of LBSs (Location-based Services), synthesizing location traces plays an increasingly important role in analyzing spatial big data while protecting users' privacy. Although location synthesizers have been widely studied, existing synthesizers do not provide utility, privacy, or scalability sufficiently, hence are not practical for large-scale location traces. To overcome this issue, we propose a novel location synthesizer called *PPMTF* (*Privacy-Preserving Multiple Tensor Factorization*). We model various statistical features of the original traces by a transition-count tensor and a visit-count tensor. We simultaneously factorize these two tensors via multiple tensor factorization, and train factor matrices via posterior sampling. Then we synthesize traces from reconstructed tensors using the MH (Metropolis-Hastings) algorithm. We comprehensively evaluate the proposed method using two datasets. Our experimental results show that the proposed method preserves various statistical features, provides plausible deniability, and synthesizes large-scale location traces in practical time. The proposed method also significantly outperforms the state-of-the-art with regard to the utility, privacy, and scalability.

1. INTRODUCTION

LBSs (Location-based Services) have been used in a variety of applications such as POI (Point-of-Interest) search, route finding, games, and geo-social networking. Consequently, a large amount of location traces (time-series location trails) have been collected into the LBS provider. The LBS provider can provide these location traces (also called spatial big data [59]) to a third party (or data analyst) to perform various types of geo-data analysis tasks; e.g., finding popular POIs [75], semantic annotation of POIs [19, 71],

modeling human mobility patterns [63, 40, 38, 17], road map inference [39, 6].

Although such geo-data analysis is important for industry and society, there are some serious privacy issues. For example, users' sensitive locations (e.g., homes, hospitals), profiles (e.g., age, profession) [43, 73, 32], or social relationship [23, 7] can be estimated from traces. Robbers or stalkers [54, 66] might also exploit location data of victims. This kind of privacy is collectively called *location privacy* [26, 55, 12], and numerous studies have been made on this issue.

Synthesizing location traces [9, 61, 15, 31, 64, 72, 35, 27] is one of the most promising approaches to perform geo-data analysis while protecting users' privacy. This approach first trains some generative model from the original traces (referred to as training traces). Then it generates synthetic traces (or dummy traces) using the trained generative model. The synthetic traces preserve some statistical features (e.g., population distribution, transition matrix) of the original traces, as these features are modeled by the generative model. Thus, based on the synthetic traces, a data analyst can perform a variety of geo-data analysis tasks explained above. In addition, the synthetic traces are (ideally) designed to provide little information about the original traces, and hence protect users' privacy from a possibly malicious data analyst.

Synthetic traces can also be used for local obfuscation in LBSs. Specifically, a user (who does not trust even the LBS provider) can send synthetic traces as dummies along with her own trace to use an LBS (e.g., POI search, route finding). If the synthetic traces look to be actual traces, the adversary cannot find out which is the user's actual trace among the traces sent to the LBS provider. Since this approach also sends the true locations (unlike adding noise, generalization, and deleting locations [60]), it does not degrade the service quality of the LBS (at the cost of some communication overhead).

Ideally, a location synthesizer should satisfy the following three features: (i) **high utility**: it synthesizes traces that preserve various statistical features of the original traces; (ii) **high privacy**: it provides little information about the original traces; (iii) **high scalability**: it generates a large amount of traces within an acceptable time; e.g., within days or weeks at most. All of these features are vitally necessary

for spatial big data analysis. They are also necessary for location obfuscation when the number of users is very large. Note that high utility is important in location obfuscation, because otherwise synthetic traces can be distinguished from real traces [9].

Although many location synthesizers [9, 61, 15, 31, 64, 72, 35, 27] have been studied, none of them are satisfactory in terms of the three features, which we explain in detail below.

Related work. Location privacy has been widely studied in the literature (see [36, 26, 55, 12] for surveys) with numerous LPPMs (Location-Privacy Protection Mechanisms); e.g., adding noise (perturbation) [5, 62, 46], location generalization [60, 25, 14], deleting locations [60, 68, 28], and synthesizing traces (adding dummies) [9, 61, 15, 31, 64, 72, 35, 27]. Synthesizing traces is promising in terms of geo-data analysis and location obfuscation, as explained above.

Although Location synthesizers have been widely studied over a decade, Bindschaedler and Shokri [9] showed most of them do not satisfactorily preserve statistical features (especially, *semantic features* of human mobility, e.g., “many people spend night at home”), and do not provide high utility.

A synthetic location traces generator in [9] (denoted by **SGLT**) is a state-of-the-art location synthesizer. **SGLT** first trains *semantic clusters*, which group locations that are semantically similar (e.g., homes, malls) from training traces. Then it generates a synthetic trace from a training trace (called a seed trace) by replacing each location with all locations in the same cluster and then sampling a trace via the Viterbi algorithm. [9] showed that **SGLT** preserves semantic features explained above and hence provides high utility.

However, **SGLT** has an issue with scalability, which is essential for spatial big data analysis. Specifically, the running time of semantic clustering in **SGLT** is quadratic in the number of training users and cubic in the number of locations. Consequently, **SGLT** cannot be used for generating large-scale traces. For example, we show that when the numbers of users and locations are about 200000 and 1000, respectively, **SGLT** would require over four years even using 1000 nodes of a supercomputer in parallel. In addition, **SGLT** uses plausible deniability using a semantic distance between two traces (introduced in [9]) as a privacy measure, and its relationship with DP (Differential Privacy) [20, 21] is unclear.

Bindschaedler *et al.* [10] proposed a synthetic data generator (denoted by **SGD**) for any kind of data using a dependency graph. However, **SGD** was not applied to location traces, and its effectiveness for traces was unclear. We apply **SGD** to location traces, and show that it does not provide high utility.

Our contributions. We design a location synthesizer with high utility, privacy, and scalability. Specifically, we propose a novel approach called *PPMTF (Privacy-Preserving Multiple Tensor Factorization)*. Our contributions are as follows:

- We propose PPMTF for synthesizing traces. PPMTF models statistical features of training traces by two tensors: a *transition-count tensor*, which contains a transition matrix for each user, and *visit-count tensor*, which represents a time-dependent population distribution. PPMTF simultaneously factorizes the two ten-

sors via MTF (Multiple Tensor Factorization) [34, 65] and trains factor matrices (parameters in our generative model) via posterior sampling [67] to provide high utility and high privacy. To our knowledge, this work is the first to propose MTF in a privacy preserving way.

- We propose a method to synthesize traces from the trained parameters using the MH (Metropolis-Hastings) algorithm [48] to make the transition matrix consistent with the time-dependent population distribution.
- We comprehensively show that the proposed method (denoted by **Proposal**) provides high utility, privacy, and scalability (for details, see below).

For utility, we show **Proposal** significantly outperforms the state-of-the-art in terms of the following statistical features.

(a) Time-dependent population distribution. The population distribution (i.e., distribution of visited locations) can be used for various geo-data analysis such as finding popular POIs [75] and semantic annotation of POIs [19, 71]. It can also be used to provide a user with the number of current visitors at a specific POI [29]. Some of these tasks are also based on the fact that the population distribution is inherently time-dependent; e.g., [71] uses the population distribution for each hour as a feature; [29] considers a scenario where the number of current diners in a nearby restaurant is sent to the user.

(b) Transition matrix. The transition matrix is a main feature for modeling human movement patterns, and is used for predicting the next POI [63] or recommending POIs [40].

(c) Distribution of visit-fractions. For semantic annotation of POIs, a distribution of visit-fractions (or visit-counts) is a key feature. For example, [19] shows that many people spend about 60% of the time at home and about 20% of the time at work/school. [71] shows that most users visit a hotel once or twice, while they may visit a restaurant for multiple times.

(d) Cluster-specific population distribution. At an individual level, a location distribution is different from user to user, and forms some clusters; e.g., those who commute by car, and those who often visit malls. The population distribution for such a cluster can be used for modeling human location patterns [38], road map inference [39, 6], and smart cities [17].

We show that **Proposal** provides all of (a)-(d), whereas **SGD** does not consider user/cluster-specific features in a practical setting, and hence does not provide (c) nor (d). We emphasize that (a)-(d) are important also for location obfuscation, because synthetic traces that do not preserve the statistical features can be distinguished from real traces [9].

For a privacy measure, we use (k, ϵ) -PD (Plausible Deniability) in [10], which has a connection with DP. We show that **Proposal** provides (k, ϵ) -PD for reasonable k and ϵ .

Regarding the scalability, for a larger number $|\mathcal{U}|$ of users and a larger number $|\mathcal{X}|$ of locations, **Proposal**’s time complexity $O(|\mathcal{U}||\mathcal{X}|^2)$ is much smaller than **SGLT**’s complexity $O(|\mathcal{U}|^2|\mathcal{X}|^3)$. [9] evaluated **SGLT** using training traces of only 30 users. In this paper, we use the Foursquare dataset in [69] (we use six cities; 448839 training users in total), and show **Proposal** generates the corresponding traces within

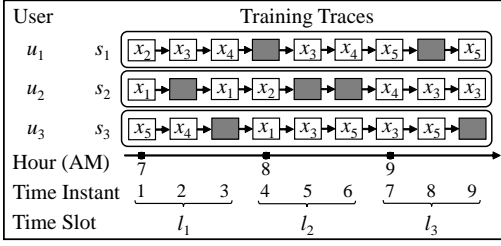


Figure 1: Training traces ($|\mathcal{U}| = 3$, $|\mathcal{X}| = 5$, $|\mathcal{T}| = 9$, $|\mathcal{L}| = 3$). Missing events are marked with gray.

60 hours (about 10^6 times faster than **SGLT**), and can also deal with a million traces.

Note that **Proposal** does not outperform **SGLT** or **SGD** in all aspects; e.g., in our experiments, **Proposal** outperforms **SGLT** with respect to (a), but is worse than **SGLT** with respect to (b); **SGD** is more scalable than **Proposal**. However, our biggest advantage is that **Proposal** is the first to provide all of the utility ((a)-(d)), privacy, and scalability to our knowledge, which makes large-scale traces generation practical.

We also implemented **Proposal** with C++, and made it public [1]. The proposed method was also used as a part of the location synthesizer for anonymization competition [2].

2. PRELIMINARIES

2.1 Notations

Let \mathbb{N} , $\mathbb{Z}_{\geq 0}$, \mathbb{R} , and $\mathbb{R}_{\geq 0}$ be the set of natural numbers, non-negative integers, real numbers, and non-negative real numbers, respectively. For $n \in \mathbb{N}$, let $[n] = \{1, 2, \dots, n\}$. For a finite set \mathcal{Z} , let \mathcal{Z}^* be the set of all finite sequences of elements of \mathcal{Z} . Let $\mathcal{P}(\mathcal{Z})$ be the power set of \mathcal{Z} , and $\mathbb{D}\mathcal{Z}$ be the set of all probability distributions over \mathcal{Z} .

We discretize locations by dividing the whole map into distinct regions or extracting frequently visited POIs (Point-of-Interests). Let \mathcal{X} be a finite set of discretized locations (i.e., regions or POIs), and $x_i \in \mathcal{X}$ be the i -th location. We also discretize time into *time instants* (e.g., by partitioning it at a regular interval such as 20 minutes or 1 hour), and represent a time instant as a natural number. Let $\mathcal{T} \subset \mathbb{N}$ be a finite set of time instants under consideration.

In addition to the time instant, we introduce a *time slot* as a time resolution in geo-data analysis; e.g., if we want to compute the time-dependent population distribution for every hour, then the length of each time slot is one hour. We represent a time slot as a set of time instants. Formally, let $\mathcal{L} \subseteq \mathcal{P}(\mathcal{T})$ be a finite set of time slots, and $l_i \in \mathcal{L}$ be the i -th time slot. In Figure 1, $l_1 = \{1, 2, 3\}$, $l_2 = \{4, 5, 6\}$, $l_3 = \{7, 8, 9\}$, and $\mathcal{L} = \{l_1, l_2, l_3\}$. The time slot can be composed of either one time instant or multiple time instants (as in Figure 1). The time slot can also be composed of separated time instants; e.g., if we set the interval between two time instants to 1 hour, and want to average the population distribution for every two hours over two days, then $l_1 = \{1, 2, 25, 26\}, \dots, l_{12} = \{23, 24, 47, 48\}$, and $\mathcal{L} = \{l_1, \dots, l_{12}\}$.

Next we formally define the notion of traces as follows. We refer to a pair of a location and a time instant as an *event*, and denote the set of all events by $\mathcal{E} = \mathcal{X} \times \mathcal{T}$. Let \mathcal{U} be a finite set of all training users, and $u_n \in \mathcal{U}$ be the

n -th training user. Then we define each trace as a pair of a user and a finite sequence of events, and denote the set of all traces by $\mathcal{R} = \mathcal{U} \times \mathcal{E}^*$. Each trace may be missing some events. Without loss of generality, we assume that each training user has provided a single training trace (if a user provides multiple temporally-separated traces, we can concatenate them into a single trace by regarding events between the traces as missing). Let $\mathcal{S} \subseteq \mathcal{R}$ be the finite set of all training traces, and $s_n \in \mathcal{S}$ be the n -th training trace (i.e., training trace of u_n).

Figure 1 shows an example of training traces; e.g., $s_1 = (u_1, (x_2, 1), (x_3, 2), (x_4, 3), (x_3, 5), (x_4, 6), (x_5, 7), (x_5, 9))$, $\mathcal{S} = \{s_1, s_2, s_3\}$. We can also deal with a situation in which a user is in multiple regions in the same interval between two time instants. For example, assume that user u_4 visits x_1 at 7:00, x_2 at 7:10, and x_2 at 7:20. If we set the length of each time interval to 20 minutes as in Figure 1, then the training trace s_4 of u_4 can be expressed (by rounding down minutes to a multiple of 20) as follows: $s_4 = (u_4, (x_1, 1), (x_2, 1), (x_2, 2))$.

We train parameters of a generative model (e.g., semantic clusters in [9], MTF parameters in the proposed method) from training traces, and use the model to synthesize a trace. As with [9], we assume that, given a user u_n 's training trace s_n , the trained generative model outputs a synthetic trace that resembles s_n , while protecting the privacy of u_n . We denote by $y \in \mathcal{R}$ a synthetic trace, and by $\mathcal{M} : \mathcal{S} \rightarrow \mathbb{D}\mathcal{R}$ a probabilistic generative model that, given a training trace s_n , outputs a synthetic trace y with probability $p(y = \mathcal{M}(s_n))$.

In Appendix A, we also show the basic notations in Table 2.

2.2 Privacy Measures

Here we introduce DP (Differential Privacy) [20, 21] and PD (Plausible Deniability) [9, 10] as privacy measures.

Differential Privacy. We define the notion of neighboring data sets in the same way as [21, 67, 41] as follows. Let $\mathcal{S}, \mathcal{S}' \subseteq \mathcal{R}$ be two sets of training traces. We say \mathcal{S} and \mathcal{S}' are *neighboring* if they differ from each other at most one trace and consist of the same number of traces, i.e., $|\mathcal{S}| = |\mathcal{S}'|$. For example, given a trace $s'_1 \in \mathcal{R}$, $\mathcal{S} = \{s_1, s_2, s_3\}$ in Figure 1 and $\mathcal{S}' = \{s'_1, s_2, s_3\}$ are neighboring.

Then DP [20, 21] is defined as follows:

Definition 1 (ϵ -DP and (ϵ, δ) -DP). *Let $\epsilon, \delta \in \mathbb{R}_{\geq 0}$. A randomized algorithm \mathcal{F} with domain $\mathcal{P}(\mathcal{R})$ provides (ϵ, δ) -DP if for any neighboring $\mathcal{S}, \mathcal{S}' \subseteq \mathcal{R}$ and any $Z \subseteq \text{Range}(\mathcal{F})$,*

$$p(\mathcal{F}(\mathcal{S}) \in Z) \leq e^\epsilon p(\mathcal{F}(\mathcal{S}') \in Z) + \delta. \quad (1)$$

If $\delta = 0$, we abbreviate (ϵ, δ) -DP as ϵ -DP.

Intuitively, ϵ -DP guarantees that an adversary who has observed the output of \mathcal{F} cannot determine, for any pair of \mathcal{S} and \mathcal{S}' , whether it comes from \mathcal{S} or \mathcal{S}' (i.e., a particular user's trace is included in the training trace set) with a certain degree of confidence. As the privacy budget ϵ approaches to 0, \mathcal{S} and \mathcal{S}' become almost equally likely, which means that a user's privacy is strongly protected. (ϵ, δ) -DP is a relaxation of ϵ -DP that allows for deviating from ϵ -DP with probability δ .

Plausible Deniability. The notion of PD was originally introduced by Bindschaedler and Shokri [9] to quantify how well a trace $y \in \mathcal{R}$ synthesized from a generative model

\mathcal{M} provides privacy for the input training trace. However, PD in [9] was defined using a semantic distance between traces, and its relationship with DP was unclear. Later, Bindschaedler *et al.* [10] modified PD to clarify the relationship between PD and DP. In this paper, we use the definition of PD in [10]:

Definition 2 $((k, \varepsilon)$ -PD). Let $k \in \mathbb{N}$ and $\varepsilon \in \mathbb{R}_{\geq 0}$. Let $d_1 \in [\mathcal{U}]$ be a training user index. For a training trace set \mathcal{S} with $|\mathcal{S}| \geq k$, a synthetic trace $y \in \mathcal{R}$ output by a generative model \mathcal{M} with an input training trace $s_{d_1} \in \mathcal{S}$ is releasable with (k, ε) -PD if there exist at least $k - 1$ distinct training user indexes $d_2, \dots, d_k \in [\mathcal{U}] \setminus \{d_1\}$ such that for any $i, j \in [k]$,

$$e^{-\varepsilon} p(y = \mathcal{M}(s_{d_j})) \leq p(y = \mathcal{M}(s_{d_i})) \leq e^{\varepsilon} p(y = \mathcal{M}(s_{d_j})). \quad (2)$$

Note that [10] uses $\gamma \in [1, \infty)$ instead of e^ε ; i.e., (k, ε) -PD in Definition 2 is identical to (k, γ) -PD in [10], where $\gamma = e^\varepsilon$.

Intuitively, (k, ε) -PD in Definition 2 guarantees that the input training trace $s_{d_1} \in \mathcal{S}$ is indistinguishable from at least $k - 1$ other training traces $s_{d_2}, \dots, s_{d_k} \in \mathcal{S}$ out of $|\mathcal{U}| - 1$ other training traces. Note that (k, ε) -PD is totally different from k -anonymity, as discussed in [9, 10]. k -anonymity is vulnerable to attribute inference [42] or location inference [60] by an adversary with some background knowledge, whereas (k, ε) -PD does not depend on the background knowledge [10].

PD is a privacy measure for an adversary who obtains synthetic traces, whereas the parameters of the generative model \mathcal{M} might also leak some information about the training trace set \mathcal{S} . However, it should be noted that this can be prevented by keeping secret the parameters of \mathcal{M} (or discarding the parameters after synthesizing traces). In fact, a location synthesizer in [60] outputs only synthetic traces, and does not output the parameters of \mathcal{M} (i.e., semantic clusters) computed from \mathcal{S} . Similarly, we consider a location synthesizer that outputs only synthetic traces and keeps secret the parameters of \mathcal{M} (or discarding them after synthesizing traces).

3. PRIVACY-PRESERVING MULTIPLE TENSOR FACTORIZATION (PPMTF)

We propose PPMTF (Privacy-Preserving Multiple Tensor Factorization) for synthesizing location traces. We first describe its overview (Section 3.1). We then explain the computation of two tensors from training traces (Section 3.2), the training of MTF parameters from the two tensors (Section 3.3), and the synthesis of traces from the MTF parameters (Section 3.4). We finally prove the DP (Differential Privacy) of PPMTF, and introduce the PD (Plausible Deniability) test (Section 3.5).

3.1 Overview

Proposed method. Figure 2 shows the overview of the proposed method. It is composed of the following five steps.

- (i). We compute a transition-count tensor and visit-count tensor from a training trace set \mathcal{S} (Sections 3.2).

The transition-count tensor is composed of the “User,” “Location,” and “Next Location” modes, and its (n, i, j) -th element contains a transition-count of user $u_n \in \mathcal{U}$ from location $x_i \in \mathcal{X}$ to $x_j \in \mathcal{X}$. In other words, this

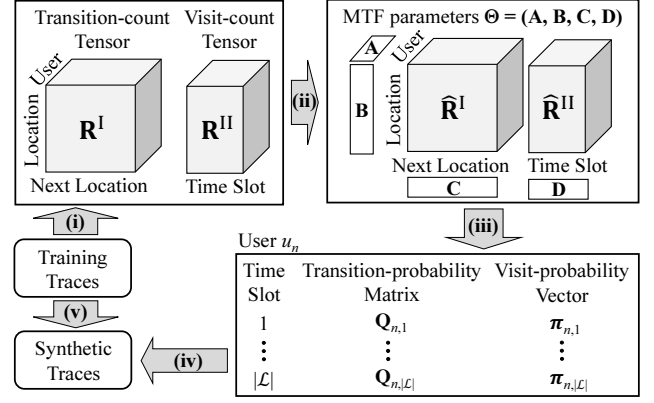


Figure 2: Overview of the proposed method with the following five steps: (i) computing a transition-count tensor and visit-count tensor, (ii) training MTF parameters via posterior sampling, (iii) computing a transition-probability matrix and visit-probability vector for each user and time slot via the MH algorithm, (iv) synthesizing traces, and (v) the PD test.

tensor represents the *movement pattern* of each training user in the form of transition-counts.

The visit-count tensor is composed of the “User,” “Location,” and “Time Slot” modes, and the (n, i, j) -th element contains a visit-count of user u_n at location x_i in time slot $l_j \in \mathcal{L}$. In other words, this tensor contains a *histogram of visited locations* for each user and each time slot.

- (ii). We share the “User” and “Location” modes between the two tensors, and perform MTF (Multiple Tensor Factorization) [34, 65] for the two tensors. For a tensor factorization model, we use the CP decomposition [16] in the same way as [34, 65]. The CP decomposition factorizes a tensor into low-rank matrices called factor matrices along each mode. Since we share the “User” and “Location” modes, we factorize the two tensors into four factor matrices as in Figure 2 (Section 3.3).

Formally, let $z \in \mathbb{N}$ be the number of columns (factors) in each matrix, and $A \in \mathbb{R}^{|\mathcal{U}| \times z}$, $B \in \mathbb{R}^{|\mathcal{X}| \times z}$, $C \in \mathbb{R}^{|\mathcal{X}| \times z}$, and $D \in \mathbb{R}^{|\mathcal{L}| \times z}$ be the factor matrices, which correspond to the “User,” “Location,” “Next Location,” and “Time Slot” mode, respectively. A , B , C , and D are the MTF parameters. Typically, the number of columns is much smaller than the numbers of users and locations; i.e., $z \ll \min(|\mathcal{U}|, |\mathcal{X}|)$. In our experiments, we set $z = 16$ as in [47]. Let $\Theta = (A, B, C, D)$ be the tuple of MTF parameters. We train MTF parameters Θ from the two tensors via posterior sampling [67]. The MTF parameters are used as parameters of our generative model.

- (iii). Given a training trace $s_n \in \mathcal{S}$, we compute a transition-probability matrix and visit-probability vector of the corresponding user $u_n \in \mathcal{U}$ for each time slot. We compute them from the MTF parameters Θ via the MH (Metropolis-Hastings) algorithm [48] (Section 3.4).

- (iv). We generate a synthetic trace $y \in \mathcal{R}$ that resembles the training trace s_n of user u_n (Section 3.4).
- (v). We finally perform the PD test, which verifies whether y is releasable with (k, ε) -PD (Section 3.5).

The main advantages of the proposed method are high utility, privacy, and scalability.

Utility. First, the proposed method achieves high utility by modeling statistical features of training traces using two tensors. Specifically, the transition-count tensor represents the movement pattern of each user in the form of transition-counts, whereas the visit-count tensor contains a histogram of visited locations for each user and time slot. Consequently, our synthetic traces preserve statistical features, e.g., a transition matrix, a time-dependent population distribution, and a distribution of visit-counts per location. These are key features for various geo-data analyses, e.g., modeling human movement patterns [63, 40] or location patterns [38, 17], finding popular POIs [75], and semantic annotation of POIs [19, 71].

Furthermore, the proposed method automatically finds users who have similar behavior (e.g., those who always stay in Manhattan, and those who often visit universities) and locations that are semantically similar (e.g., restaurants, parks), as factor matrices in tensor factorization represent clusters [16] (see [47, 65] for examples of location data). Consequently, our synthetic traces preserve the mobility behavior of similar users and the semantics of similar locations. They are also useful for various geo-data analysis (e.g., modeling human location or movement patterns, road map inference [39, 6], semantic annotation of POIs). In Section 4, we visualize how well similar users and similar locations are clustered.

The proposed method also addresses the sparseness of the tensors by sharing factor matrices \mathbf{A} and \mathbf{B} . In Appendix E, we show that the utility is improved by sharing \mathbf{A} and \mathbf{B} .

Privacy. Second, the proposed method achieves high privacy by training the MTF parameters via posterior sampling. As shown in [67], posterior sampling-based Bayesian learning algorithms provide DP “for free” (without additional noise) by producing a sample from a posterior distribution given a dataset. We utilize this fact, and sample the MTF parameters from a posterior distribution given a training trace set \mathcal{S} .

A major issue in differentially private matrix/tensor factorization is that the privacy budget ε can be very large in practice. This follows from the fact that ε increases with increase in the number of observed elements per user, and with increase in the maximum value of elements. For example, Liu *et al.* [41] applied posterior sampling to matrix factorization, and reported that it needs $\varepsilon = 250$ to achieve high utility. It is important to note, however, that DP guarantees indistinguishability for all possible users including the one whose elements are completely different from normal users; e.g., a malicious user who provides a value completely opposite from what the model would predict for all elements, as pointed out in [41]. Obviously, it is not necessary for the input training trace to be indistinguishable from such anomaly traces.

Thus we use PD as a privacy measure in the same way as [9, 10]. In other words, we guarantee that the input training trace is indistinguishable from some traces that would

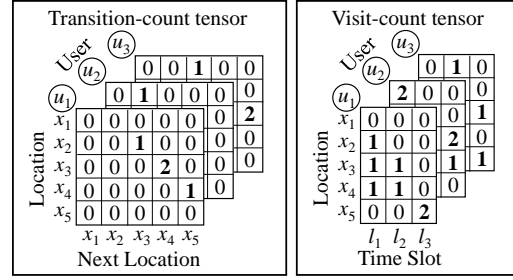


Figure 3: Two tensors computed from the training traces in Figure 1 ($|\mathcal{U}| = 3$, $|\mathcal{X}| = 5$, $|\mathcal{T}| = 9$, $|\mathcal{L}| = 3$).

appear in practice. In our experiments, we show that the proposed method provides (k, ε) -PD for reasonable k and ε .

Scalability. Finally, the proposed method achieves much higher scalability than the location synthesizer in [9]. Specifically, the time complexity of [9] (semantic clustering) is $O(|\mathcal{U}|^2 |\mathcal{X}|^3 |\mathcal{L}|)$, which is very large for training traces with large $|\mathcal{U}|$ and $|\mathcal{X}|$. On the other hand, the time complexity of the proposed method is $O(|\mathcal{U}| |\mathcal{X}|^2 |\mathcal{L}|)$, which is much smaller than the synthesizer in [9] (see Appendix B for details). In our experiments, we evaluate the running time of the proposed method and the synthesizer in [9], and show that our method can be applied to much larger-scale training datasets.

3.2 Computation of Two Tensors

We now explain how to compute two tensors from a training trace set \mathcal{S} (i.e., step (i)) in detail.

Two tensors. Figure 3 shows an example of the two tensors computed from the training traces in Figure 1.

The transition-count tensor contains a transition-count matrix for each user. Let $\mathbf{R}^I \in \mathbb{Z}_{\geq 0}^{|\mathcal{U}| \times |\mathcal{X}| \times |\mathcal{X}|}$ be the transition-count tensor, and $r_{n,i,j}^I \in \mathbb{Z}_{\geq 0}$ be its (n, i, j) -th element. For example, $r_{1,3,4}^I = 2$ in Figure 3, since two transitions from x_3 to x_4 are observed in the training trace s_1 of u_1 in Figure 1.

The visit-count tensor contains a histogram of visited locations for each user and each time slot. Let $\mathbf{R}^{II} \in \mathbb{Z}_{\geq 0}^{|\mathcal{U}| \times |\mathcal{X}| \times |\mathcal{L}|}$ be the visit-count tensor, and $r_{n,i,j}^{II} \in \mathbb{Z}_{\geq 0}$ be its (n, i, j) -th element. For example, $r_{1,5,3}^{II} = 2$ in Figure 3, as u_1 visits x_5 twice in l_3 (i.e., from time instant 7 to 9) in Figure 1.

Let $\mathbf{R} = (\mathbf{R}^I, \mathbf{R}^{II})$. Typically, \mathbf{R}^I and \mathbf{R}^{II} are sparse; i.e., many elements are zeros. In particular, \mathbf{R}^I can be extremely sparse for large $|\mathcal{X}|$, as its size $|\mathbf{R}^I|$ is quadratic in $|\mathcal{X}|$.

Trimming. For both tensors, we randomly delete positive elements of users who have provided much more positive elements than the average (i.e., outliers) in the same way as [41]. This is called *trimming*, and is effective for matrix completion [33]. It is also necessary to provide DP [41]. Similarly, we also set the maximum value of counts for each element, and truncate counts that exceed the maximum number.

Specifically, let $\lambda^I, \lambda^{II} \in \mathbb{N}$ be the maximum numbers of positive elements per user in \mathbf{R}^I and \mathbf{R}^{II} , respectively. Typically, $\lambda^I \ll |\mathcal{X}| \times |\mathcal{X}|$ and $\lambda^{II} \ll |\mathcal{X}| \times |\mathcal{L}|$. For each user, if the number of positive elements in \mathbf{R}^I exceeds λ^I , then we randomly select λ^I elements from all positive elements, and delete the remaining positive elements. Similarly, we randomly delete extra positive elements in \mathbf{R}^{II} . In addition, let $r_{max}^I, r_{max}^{II} \in \mathbb{N}$ be the maximum counts for each element

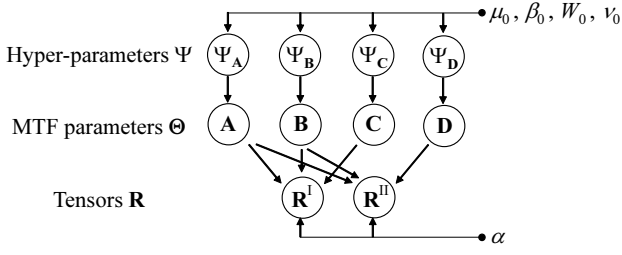


Figure 4: Graphical model of the proposed method.

in \mathbf{R}^I and \mathbf{R}^{II} , respectively. For each element, we truncate $r_{n,i,j}^I$ to r_{max}^I if $r_{n,i,j}^I > r_{max}^I$ (resp. $r_{n,i,j}^{II}$ to r_{max}^{II} if $r_{n,i,j}^{II} > r_{max}^{II}$).

In our experiments, we set $\lambda^I = \lambda^{II} = 10^2$ (as in [41]), and $r_{max}^I = r_{max}^{II} = 10$, since the number of positive elements per user and the value of counts were less than 100 and 10, respectively, in most cases.

3.3 Training MTF Parameters via Posterior Sampling

After computing the tensors $\mathbf{R} = (\mathbf{R}^I, \mathbf{R}^{II})$, we train the MTF parameters $\Theta = (\mathbf{A}, \mathbf{B}, \mathbf{C}, \mathbf{D})$ via posterior sampling (i.e., step (ii)). Below we describe our MTF model and the training.

Model. Let $a_{i,k}, b_{i,k}, c_{i,k}, d_{i,k} \in \mathbb{R}$ be the (i, k) -th elements of $\mathbf{A}, \mathbf{B}, \mathbf{C}$, and \mathbf{D} , respectively. In addition, let $\hat{\mathbf{R}}^I \in \mathbb{R}^{|\mathcal{U}| \times |\mathcal{X}| \times |\mathcal{X}|}$ and $\hat{\mathbf{R}}^{II} \in \mathbb{R}^{|\mathcal{U}| \times |\mathcal{X}| \times |\mathcal{L}|}$ be the approximation of \mathbf{R}^I and \mathbf{R}^{II} by the proposed method, respectively, and $\hat{r}_{n,i,j}^I \in \mathbb{R}$ and $\hat{r}_{n,i,j}^{II} \in \mathbb{R}$ be their (n, i, j) -th elements. Then $\hat{\mathbf{R}}^I$ and $\hat{\mathbf{R}}^{II}$ are given by:

$$\hat{r}_{n,i,j}^I = \sum_{k \in [z]} a_{n,k} b_{i,k} c_{j,k} \quad \text{and} \quad \hat{r}_{n,i,j}^{II} = \sum_{k \in [z]} a_{n,k} b_{i,k} d_{j,k}, \quad (3)$$

where the matrices \mathbf{A} and \mathbf{B} are shared between \mathbf{R}^I and \mathbf{R}^{II} .

For MTF parameters Θ , we assume a hierarchical Bayes model [57], since it outperforms the non-hierarchical one [56] in terms of the model's predictive accuracy. Figure 4 shows a graphical model of the proposed method. For the conditional distribution $p(\mathbf{R}|\Theta)$ of the two tensors $\mathbf{R} = (\mathbf{R}^I, \mathbf{R}^{II})$ given the MTF parameters $\Theta = (\mathbf{A}, \mathbf{B}, \mathbf{C}, \mathbf{D})$, we assume that each element $r_{n,i,j}^I$ (resp. $r_{n,i,j}^{II}$) is independently generated from a normal distribution with mean $\hat{r}_{n,i,j}^I$ (resp. $\hat{r}_{n,i,j}^{II}$) and precision $\alpha \in \mathbb{R}_{\geq 0}$ (ranging over [0.5, 1000] in our experiments later).

Here it is important to note that each element in \mathbf{R} contains a transition/visit count, and such a count is called *implicit feedback* [3, 30] (e.g., purchasing quantities in item recommendation). Unlike the explicit feedback dataset that contains negative values (e.g., integer ratings in $[-2, 2]$), zero elements in the implicit feedback dataset should be treated as 0s rather than missing elements to avoid overfitting [3]. However, the treatment of all zero elements as 0s results in a high computational cost, especially for large tensors.

We overcome the computational issue by randomly sampling a small number of zero elements and treating them as 0s [3, 51]. Specifically, we randomly sample $\rho^I \in \mathbb{N}$ and $\rho^{II} \in \mathbb{N}$ zero elements for each user in \mathbf{R}^I and \mathbf{R}^{II} , respectively, where $\rho^I \ll |\mathcal{X}| \times |\mathcal{X}|$ and $\rho^{II} \ll |\mathcal{X}| \times |\mathcal{L}|$ (in our

experiments, we set $\rho^I = \rho^{II} = 10^3$). We treat the sampled zero elements as 0s, and the remaining zero elements as missing. Let $I_{n,i,j}^I$ (resp. $I_{n,i,j}^{II}$) be the indicator function that takes 0 if $r_{n,i,j}^I$ (resp. $r_{n,i,j}^{II}$) is missing, and takes 1 otherwise. Note that $I_{n,i,j}^I$ (resp. $I_{n,i,j}^{II}$) takes 1 at most $\lambda^I + \rho^I$ (resp. $\lambda^{II} + \rho^{II}$) elements for each user, where λ^I (resp. λ^{II}) is the maximum number of positive elements per user in \mathbf{R}^I (resp. \mathbf{R}^{II}).

Then the distribution $p(\mathbf{R}|\Theta)$ can be written as follows:

$$\begin{aligned} p(\mathbf{R}|\Theta) &= p(\mathbf{R}^I|\mathbf{A}, \mathbf{B}, \mathbf{C})p(\mathbf{R}^{II}|\mathbf{A}, \mathbf{B}, \mathbf{D}) \\ &= \prod_{n,i,j} [\mathcal{N}(r_{n,i,j}^I|\hat{r}_{n,i,j}^I, \alpha^{-1})]^{I_{n,i,j}^I} \cdot \prod_{n,i,j} [\mathcal{N}(r_{n,i,j}^{II}|\hat{r}_{n,i,j}^{II}, \alpha^{-1})]^{I_{n,i,j}^{II}} \end{aligned} \quad (4)$$

where $\mathcal{N}(r|\mu, \alpha^{-1})$ denotes the probability of r in the normal distribution with mean μ and precision α (i.e., variance α^{-1}).

Let $\mathbf{a}_i, \mathbf{b}_i, \mathbf{c}_i, \mathbf{d}_i \in \mathbb{R}^z$ be the i -th rows of $\mathbf{A}, \mathbf{B}, \mathbf{C}$, and \mathbf{D} , respectively. Then, for the distribution of $\Theta = (\mathbf{A}, \mathbf{B}, \mathbf{C}, \mathbf{D})$, we assume the multivariate normal distribution:

$$\begin{aligned} p(\mathbf{A}|\Psi_{\mathbf{A}}) &= \prod_n \mathcal{N}(\mathbf{a}_n|\mu_{\mathbf{A}}, \Lambda_{\mathbf{A}}^{-1}), \quad p(\mathbf{B}|\Psi_{\mathbf{B}}) = \prod_i \mathcal{N}(\mathbf{b}_i|\mu_{\mathbf{B}}, \Lambda_{\mathbf{B}}^{-1}), \\ p(\mathbf{C}|\Psi_{\mathbf{C}}) &= \prod_j \mathcal{N}(\mathbf{c}_j|\mu_{\mathbf{C}}, \Lambda_{\mathbf{C}}^{-1}), \quad p(\mathbf{D}|\Psi_{\mathbf{D}}) = \prod_j \mathcal{N}(\mathbf{d}_j|\mu_{\mathbf{D}}, \Lambda_{\mathbf{D}}^{-1}), \end{aligned}$$

where $\mu_{\mathbf{A}}, \mu_{\mathbf{B}}, \mu_{\mathbf{C}}, \mu_{\mathbf{D}} \in \mathbb{R}^z$ are mean vectors, $\Lambda_{\mathbf{A}}, \Lambda_{\mathbf{B}}, \Lambda_{\mathbf{C}}, \Lambda_{\mathbf{D}} \in \mathbb{R}^{z \times z}$ are precision matrices, and $\Psi_{\mathbf{A}} = (\mu_{\mathbf{A}}, \Lambda_{\mathbf{A}})$, $\Psi_{\mathbf{B}} = (\mu_{\mathbf{B}}, \Lambda_{\mathbf{B}})$, $\Psi_{\mathbf{C}} = (\mu_{\mathbf{C}}, \Lambda_{\mathbf{C}})$, $\Psi_{\mathbf{D}} = (\mu_{\mathbf{D}}, \Lambda_{\mathbf{D}})$ are called *hyper-parameters*. Let $\Psi = (\Psi_{\mathbf{A}}, \Psi_{\mathbf{B}}, \Psi_{\mathbf{C}}, \Psi_{\mathbf{D}})$.

The hierarchical Bayes model assumes some distribution for the hyper-parameters. We assume each hyper-parameter $\mathbf{Z} \in \{\mathbf{A}, \mathbf{B}, \mathbf{C}, \mathbf{D}\}$ follows a normal-Wishart distribution [11], i.e., the conjugate prior of a multivariate normal distribution:

$$\begin{aligned} p(\Psi_{\mathbf{Z}}) &= p(\mu_{\mathbf{Z}}|\Lambda_{\mathbf{Z}})p(\Lambda_{\mathbf{Z}}) \\ &= \mathcal{N}(\mu_{\mathbf{Z}}|\mu_0, (\beta_0 \Lambda_{\mathbf{Z}})^{-1}) \mathcal{W}(\Lambda_{\mathbf{Z}}|W_0, \nu_0) \end{aligned} \quad (5)$$

where $\mu_0 \in \mathbb{R}^z$, $\beta_0 \in \mathbb{R}$, and $\mathcal{W}(W_0, \nu_0)$ denotes the Wishart distribution with parameters $W_0 \in \mathbb{R}^{z \times z}$ and $\nu_0 \in \mathbb{R}$. (W_0 and ν_0 are called a scale matrix and the number of degrees of freedom, respectively). μ_0, β_0, W_0 , and ν_0 are called *hyper-hyper-parameters*, and are determined in advance. In our experiments, we set $\mu_0 = 0$, $\beta_0 = 2$, W_0 to the identity matrix, and $\nu_0 = z$ in the same way as [57].

Posterior sampling of Θ . We train the MTF parameters Θ based on the posterior sampling method [67]. This method trains Θ from \mathbf{R} by sampling Θ from the posterior distribution $p(\Theta|\mathbf{R})$. To sample Θ from $p(\Theta|\mathbf{R})$, we use the Gibbs sampling [48], which samples each variable in turn, conditioned on the current values of the other variables.

Specifically, we sample $\Psi_{\mathbf{A}}, \Psi_{\mathbf{B}}, \Psi_{\mathbf{C}}, \Psi_{\mathbf{D}}, \mathbf{A}, \mathbf{B}, \mathbf{C}$, and \mathbf{D} in turn. We add the superscript “(t)” to these variables to denote the sampled values at the t -th iteration. For initial values with “(0)”, we use a random initialization method [4] that initializes each element as a random number in $[0, 1]$, as it is widely used. Then, we sample $\Psi_{\mathbf{A}}^{(t)}, \Psi_{\mathbf{B}}^{(t)}, \Psi_{\mathbf{C}}^{(t)}, \Psi_{\mathbf{D}}^{(t)}, \mathbf{A}^{(t)}, \mathbf{B}^{(t)}, \mathbf{C}^{(t)}$, and $\mathbf{D}^{(t)}$ from the conditional distribution given the current values of the other variables, and iterate the sampling for a fixed number of times (see Appendix G for details).

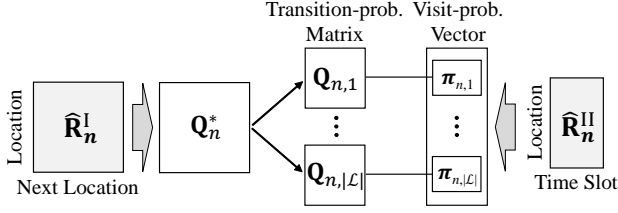


Figure 5: Computation of $(Q_{n,i}, \pi_{n,i})$ via MH. We compute Q_n^* from \hat{R}_n^I , and $\pi_{n,i}$ from \hat{R}_n^{II} . Then for each time slot $l_i \in \mathcal{L}$, we modify Q_n^* to $Q_{n,i}$ whose stationary distribution is $\pi_{n,i}$.

The Gibbs sampling guarantees that the sampling distributions of $\mathbf{A}^{(t)}, \dots, \mathbf{D}^{(t)}$ approach to the posterior distributions $p(\mathbf{A}|\mathbf{R}), \dots, p(\mathbf{D}|\mathbf{R})$ as t increases, and hence $\Theta^{(t)} = (\mathbf{A}^{(t)}, \mathbf{B}^{(t)}, \mathbf{C}^{(t)}, \mathbf{D}^{(t)})$ approximates Θ sampled from the posterior distribution $p(\Theta|\mathbf{R})$ for large t . In our experiments, we discarded the first 99 samples as “burn-in”, and used $\Theta^{(100)}$ as an approximation of Θ . We also confirmed that the model’s predictive accuracy was converged within 100 iterations.

3.4 Generating Traces via MH

After training the MTF parameters Θ from the tensors \mathbf{R} , we generate synthetic traces via the MH (Metropolis-Hastings) algorithm [48] (i.e., steps (iii) and (iv)). Here we explain how to, given a training trace $s_n \in \mathcal{S}$, generate a synthetic trace $y \in \mathcal{R}$ that resembles s_n of user $u_n \in \mathcal{U}$.

Let \mathcal{Q} be the set of $|\mathcal{X}| \times |\mathcal{X}|$ transition-probability matrices, and \mathcal{C} be the set of $|\mathcal{X}|$ -dimensional probability vectors (i.e., probability simplex). Given a transition-probability matrix $\mathbf{Q} \in \mathcal{Q}$ and a probability vector $\pi \in \mathcal{C}$, the MH algorithm modifies \mathbf{Q} to $\mathbf{Q}' \in \mathcal{Q}$ so that the stationary distribution of \mathbf{Q}' is equal to π . Note that \mathbf{Q} is a conditional distribution called a *proposal distribution*, and π is called a *target distribution*.

In the step (iii), given s_n , we reconstruct the transition-count matrix and visit-count matrix of user u_n (note that u_n is included in s_n), and use the MH algorithm to make a transition-probability matrix of u_n consistent with a visit-probability vector of u_n for each time slot. Figure 5 shows its overview. Specifically, let $\hat{\mathbf{R}}_n^I \in \mathbb{R}^{|\mathcal{X}| \times |\mathcal{X}|}$ and $\hat{\mathbf{R}}_n^{II} \in \mathbb{R}^{|\mathcal{X}| \times |\mathcal{L}|}$ be the n -th matrices in $\hat{\mathbf{R}}^I$ and $\hat{\mathbf{R}}^II$, respectively (i.e., reconstructed transition-count matrix and visit-count matrix of user u_n). We first compute $\hat{\mathbf{R}}_n^I$ and $\hat{\mathbf{R}}_n^{II}$ from Θ by (3). Then we compute a transition-probability matrix $Q_n^* \in \mathcal{Q}$ of user u_n from $\hat{\mathbf{R}}_n^I$ by normalizing counts to probabilities. Similarly, we compute a visit-probability vector $\pi_{n,i} \in \mathcal{C}$ of user u_n for each time slot $l_i \in \mathcal{L}$ from $\hat{\mathbf{R}}_n^{II}$ by normalizing counts to probabilities. Then, for each time slot $l_i \in \mathcal{L}$, we modify Q_n^* to $Q_{n,i} \in \mathcal{Q}$ via the MH algorithm so that the stationary distribution of $Q_{n,i}$ is equal to $\pi_{n,i}$. In the subsequent step (iv), we generate a synthetic trace using $(Q_{n,i}, \pi_{n,i})$.

Computing $(Q_{n,i}, \pi_{n,i})$ via MH. We first compute the n -th matrix $\hat{\mathbf{R}}_n^I \in \mathbb{R}^{|\mathcal{X}| \times |\mathcal{X}|}$ in $\hat{\mathbf{R}}^I$ from Θ by (3), and then compute $Q_n^* \in \mathcal{Q}$ from $\hat{\mathbf{R}}_n^I$ by normalizing counts to probabilities as follows. We assign a very small positive value δ ($\delta = 10^{-8}$ in our experiments) to elements in $\hat{\mathbf{R}}_n^I$ whose values are smaller than δ , and then normalize $\hat{\mathbf{R}}_n^I$ to Q_n^*

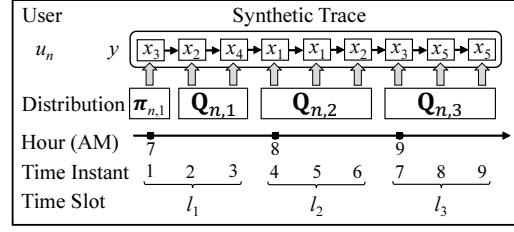


Figure 6: Generation of a synthetic trace ($|\mathcal{X}| = 5$, $|\mathcal{T}| = 9$, $|\mathcal{L}| = 3$). The gray arrow represents that a location is randomly generated from a distribution in the same time slot.

so that the sum over each row in Q_n^* is 1. Since we assign δ ($= 10^{-8}$) to elements with smaller values in $\hat{\mathbf{R}}_n^I$, the transition-probability matrix Q_n^* is *regular* [48]; i.e., it is possible to get from any location to any location in one step. This allows $\pi_{n,i}$ to be the stationary distribution of $Q_{n,i}$, as explained later in detail.

We then compute the n -th matrix $\hat{\mathbf{R}}_n^{II} \in \mathbb{R}^{|\mathcal{X}| \times |\mathcal{L}|}$ in $\hat{\mathbf{R}}^{II}$ from Θ by (3). For each time slot $l_i \in \mathcal{L}$, we assign δ ($= 10^{-8}$) to elements with smaller values in $\hat{\mathbf{R}}_n^{II}$, and then normalize the i -th column of $\hat{\mathbf{R}}_n^{II}$ to $\pi_{n,i} \in \mathcal{C}$ so that the sum of $\pi_{n,i}$ is one.

We use Q_n^* as a proposal distribution and $\pi_{n,i}$ as a target distribution, and apply the MH algorithm to obtain a transition-probability matrix $Q_{n,i}$ whose stationary distribution is $\pi_{n,i}$. For $\mathbf{Q} \in \mathcal{Q}$ and $a, b \in [|\mathcal{X}|]$, we denote by $Q(b|x_a) \in [0, 1]$ the transition probability from $x_a \in \mathcal{X}$ to $x_b \in \mathcal{X}$ (i.e., the (a, b) -th element of \mathbf{Q}). Similarly, given $\pi \in \mathcal{C}$, we denote by $\pi(x_a) \in [0, 1]$ the visit probability at $x_a \in \mathcal{X}$. Then, the MH algorithm computes $Q_{n,i}(x_b|x_a)$ for $x_a \neq x_b$ as follows:

$$Q_{n,i}(x_b|x_a) = Q_n^*(x_b|x_a) \min\left(1, \frac{\pi_{n,i}(x_b)Q_n^*(x_a|x_b)}{\pi_{n,i}(x_a)Q_n^*(x_b|x_a)}\right), \quad (6)$$

and computes $Q_{n,i}(x_a|x_a)$ as follows: $Q_{n,i}(x_a|x_a) = 1 - \sum_{b \neq a} Q_{n,i}(x_b|x_a)$. Note that $Q_{n,i}$ is *regular*, as all elements in Q_n^* and $\pi_{n,i}$ are positive. Then the MH algorithm guarantees that $\pi_{n,i}$ is a stationary distribution of $Q_{n,i}$ [48].

Generating traces. After computing $(Q_{n,i}, \pi_{n,i})$ via the MH algorithm, we synthesize a trace $y \in \mathcal{R}$ of user u_n as follows. We first randomly generate the first location at time slot l_1 from the visit-probability distribution $\pi_{n,1}$. Then we randomly generate the subsequent location at time slot l_i using the transition-probability matrix $Q_{n,i}$. Figure 6 shows an example of synthesizing a trace y of user u_n , where a location at time instant 7 is randomly generated from the conditional distribution $Q_{n,3}$ given the location x_2 at time instant 6.

The synthetic trace y is generated in such a way that a visit probability in time slot l_i is given by $\pi_{n,i}$. In addition, the transition matrix is computed by using Q_n^* as a proposal distribution. Therefore, we can synthesize traces that preserve the statistical feature of training traces such as the time-dependent population distribution and the transition matrix.

3.5 Privacy Protection

Here we prove the DP of PPMTF, and describe the PD test.

DP of PPMTF. Since we train the MTF parameters Θ via posterior sampling, the training algorithm provides DP for free (without additional noise).

Specifically, let \mathcal{F}_{PPMTF} be our training algorithm in the step (ii), which takes as input the training trace set \mathcal{S} and outputs the MTF parameters Θ . Recall that the maximum counts in \mathbf{R}^I and \mathbf{R}^{II} are r_{max}^I and r_{max}^{II} , respectively, as defined in Section 3.2. Let $\kappa \in \mathbb{R}_{\geq 0}$ satisfy that $\hat{r}_{n,i,j}^I \in [-\kappa, r_{max}^I + \kappa]$ and $\hat{r}_{n,i,j}^{II} \in [-\kappa, r_{max}^{II} + \kappa]$ for each n, i, j . κ can be made small by iterating the sampling of Θ until we find Θ with small κ [41]. In addition, assume that Θ is sampled from the exact posterior distribution $p(\Theta|\mathbf{R})$. Then we obtain:

Proposition 1. \mathcal{F}_{PPMTF} provides ε -DP, where

$$\varepsilon = \alpha \left((\lambda^I + \rho^I)(r_{max}^I + \kappa)^2 + (\lambda^{II} + \rho^{II})(r_{max}^{II} + \kappa)^2 \right).$$

See Appendix C for the proof. Since a trace y is synthesized from Θ after \mathcal{F}_{PPMTF} outputs Θ , all synthetic traces provide ε -DP thanks to the immunity to post-processing [21].

However, ε can be very large in practice. Both the number of observed elements per user and the maximum value of elements with increase in the length of the training traces. For example, we set $\alpha \geq 0.5$, $\lambda^I = \lambda^{II} = 10^2$, $\rho^I = \rho^{II} = 10^3$, and $r_{max}^I = r_{max}^{II} = 10$ in our experiments, and consequently ε is larger than 10^5 . We emphasize again that DP guarantees that the input training trace is indistinguishable from all possible traces including anomaly traces. Thus we use PD as a privacy measure, and perform the PD test as follows.

PD test. We perform the PD test to guarantee (k, ε) -PD in Definition 2 for synthetic traces.

Let $\mathcal{M}_{PPMTF} : \mathcal{S} \rightarrow \mathbb{DR}$ be our generative model in the steps (iii) and (iv), which maps a training trace $s_n \in \mathcal{S}$ to a synthetic trace $y \in \mathcal{R}$ with probability $p(y = \mathcal{M}_{PPMTF}(s_n))$. Let $\sigma : \mathcal{T} \rightarrow \mathcal{X}$ be a function that, given time instant $t \in \mathcal{T}$, outputs an index of the location at time instant t in y ; e.g., $\sigma(1) = 3, \sigma(2) = 2, \dots, \sigma(9) = 5$ in Figure 6. Furthermore, let $\omega : \mathcal{T} \rightarrow \mathcal{L}$ be a function that, given time instant $t \in \mathcal{T}$, outputs an index of the corresponding time slot; e.g., $\omega(1) = \omega(2) = \omega(3) = 1, \dots, \omega(7) = \omega(8) = \omega(9) = 3$ in Figure 6.

Recall that the first location in y is randomly generated from $\pi_{n,1}$, and the subsequent location at time instant $t \in \mathcal{T}$ is randomly generated from $\mathbf{Q}_{n,\omega(t)}$. Thus we obtain:

$$p(y = \mathcal{M}_{PPMTF}(s_n)) = \pi_{n,1}(x_{\sigma(1)}) \prod_{t=2}^{|\mathcal{T}|} \mathbf{Q}_{n,\omega(t)}(x_{\sigma(t)} | x_{\sigma(t-1)}).$$

Hence, given $y \in \mathcal{R}$, we can compute $p(y = \mathcal{M}_{PPMTF}(s_m))$ for any $s_m \in \mathcal{S}$ as follows: (i) compute $(\mathbf{Q}_{m,i}, \pi_{m,i})$ for each time slot $i \in \mathcal{L}$ via the MH algorithm (as described in Section 3.4); (ii) compute $p(y = \mathcal{M}_{PPMTF}(s_m))$. Then, we can verify whether y is releasable with (k, ε) -PD by counting the number of training traces such that (2) holds for each other.

For example, we can perform the following PD test in [10]:

Privacy Test 1 (Deterministic Test in [10]). *Let $k \in \mathbb{N}$ and $\varepsilon \in \mathbb{R}_{\geq 0}$. Given a training trace set \mathcal{S} , input training trace s_n , and synthetic trace y , output pass or fail as follows:*

1. Let $i \in \mathbb{Z}_{\geq 0}$ be a non-negative integer that satisfies:

$$e^{-(i+1)\varepsilon} < p(y = \mathcal{M}_{PPMTF}(s_n)) \leq e^{-i\varepsilon}. \quad (7)$$

2. Let $k' \in \mathbb{Z}_{\geq 0}$ be the number of traces $s_m \in \mathcal{S}$ such that:

$$e^{-(i+1)\varepsilon} < p(y = \mathcal{M}_{PPMTF}(s_m)) \leq e^{-i\varepsilon}. \quad (8)$$

3. If $k' \geq k$, then return pass, otherwise return fail.

It is easy to check by (2), (7), and (8) that if y passes **Privacy Test 1**, then y is releasable with (k, ε) -PD. In addition, (k, ε) -PD is guaranteed even if Θ is *not* sampled from the exact posterior distribution $p(\Theta|\mathbf{R})$ (unlike ε -DP). The time complexity of **Privacy Test 1** is linear in $|\mathcal{U}|$.

In this paper, we randomly select a subset $\mathcal{S}^* \subseteq \mathcal{S}$ of training traces from \mathcal{S} (as in [10]) to check faster whether $k' \geq k$ or not. Specifically, we initialize k' to 0, and check (8) for each training trace in $\mathcal{S}^* \cup \{s_n\}$ (increment k' if (8) holds). If $k' \geq k$, then we return pass (otherwise, return fail). Let $\mathcal{U}^* \subseteq \mathcal{U}$ be the set of training users corresponding to \mathcal{S}^* . Then the time complexity of this faster version of **Privacy Test 1** is linear in $|\mathcal{U}^*|$ ($\leq |\mathcal{U}|$). A lower value of $|\mathcal{U}^*|$ leads to a faster (k, ε) -PD test at the expense of fewer synthetic traces passing the test (and hence the loss of utility). In Section 4, we use the faster version of **Privacy Test 1** with $|\mathcal{U}^*| = 32000$, $k = 10$, and $\varepsilon = 1$ (note that $\varepsilon = 1$ is considered to be reasonable in DP [22, 37]). In Appendix F, we also analyze the effect of k on the performance of the proposed method.

We can also use a randomized test [10], which adds Laplacian noise to k , to provide (ε, δ) -DP for a single synthetic trace y generated from a randomly selected input training trace s_n . However, ε and δ can be large for multiple synthetic traces from the same input training trace (as discussed in [10]). Thus we did not use the randomized test in our experiments.

4. EXPERIMENTAL EVALUATION

We conducted experiments to show the utility, privacy, and scalability of the proposed method.

In our experiments, we used two publicly available datasets: the SNS-based people flow data [50] and the Foursquare dataset in [69]. The former is a relatively small-scale dataset with no missing events, and is used for comparing the proposed method with two state-of-the-art synthesizers [9, 10]. The latter is recently published, and is one of the largest publicly available location datasets; e.g., much larger than [70, 13, 74, 53]. Since the location synthesizer in [9] cannot be applied to this large-scale dataset (as shown in Section 4.4), we compare the proposed method with the synthesizer in [10].

4.1 Datasets

SNS-based People Flow Data. The SNS-based people flow data [50] (denoted by **PF**) contains artificial traces around the Tokyo metropolitan area. The traces were generated from real geo-tagged tweets by interpolating locations every five minutes using railway and road information [58].

In our experiments, we divided the Tokyo metropolitan area into 20×20 regions; i.e., $|\mathcal{X}| = 400$. Then we set the interval between two time instants to 20 minutes, and extracted traces from 9:00 to 19:00 for 1000 users (each user has a single trace comprising 30 events). We also set time slots to 20 minutes long from 9:00 to 19:00. In other words, we assumed that each time slot is composed of one time instant; i.e., $|\mathcal{L}| = 30$. We randomly divided the 1000 traces into 500 train traces and 500 testing traces; i.e., $|\mathcal{U}| = 500$.

The training traces were used for training generative models and synthesizing traces, whereas the testing traces were used for evaluating the utility.

Since the number of users is small in **PF**, we generated ten synthetic traces from each training trace (each synthetic trace is from 9:00 to 19:00) and averaged the utility and privacy results over the ten traces to stabilize the performance.

Foursquare Dataset. The Foursquare dataset (Global-scale Check-in Dataset with User Social Networks) [69] (denoted by **FS**) is a large-scale real location dataset, which contains 90048627 check-ins by 2733324 users all over the world.

In our experiments, we selected six cities with a large number of check-ins and with a cultural diversity in the same way as [69]: Istanbul (**IST**), Jakarta (**JK**), New York City (**NYC**), Kuala Lumpur (**KL**), San Paulo (**SP**), and Tokyo (**TKY**). For each city, we extracted the most popular 1000 POIs, whose number of visits from all users was the largest; i.e., $|\mathcal{X}| = 1000$. We set the interval between two time instants to 1 hour (we rounded down minutes), and assigned every 2 hours into one of 12 time slots l_1 (0 to 2AM), \dots , l_{12} (10 to 12PM) in a cyclic manner; i.e., $|\mathcal{L}| = 12$. For each city, we randomly selected 80% of traces as training traces and used the remaining traces as testing traces. The number $|\mathcal{U}|$ of users in **IST**, **JK**, **NYC**, **KL**, **SP**, and **TKY** was respectively: 219793, 83325, 52432, 51189, 42100, and 32056. There were many missing events in **FS**, as **FS** is a location check-in dataset. The number of transitions (temporally-continuous events) in the training traces of **IST**, **JK**, **NYC**, **KL**, **SP**, and **TKY** was respectively: 109027, 19592, 7471, 25563, 13151, and 47956.

In **FS**, we generated one synthetic trace for one day from each training trace, and evaluated the utility and privacy.

4.2 Location synthesizers

We evaluated the proposed method (**Proposal**), the synthetic location traces generator in [9] (**SGLT**), and the synthetic data generator in [10] (**SGD**).

In **Proposal**, we set the parameters $z = 16$, $\lambda^I = \lambda^{II} = 10^2$, $\rho^I = \rho^{II} = 10^3$, and $r_{max}^I = r_{max}^{II} = 10$, as explained in Section 3. For the hyper-hyper parameters, we set $\mu_0 = 0$, $\beta_0 = 2$, W_0 to the identity matrix, and $\nu_0 = z$ (as in [57]). Then we set the precision α to various values from 0.5 to 1000, and evaluated the utility and privacy for each value. We implemented **Proposal** with C++, and made it public [1].

In **SGLT** [9], we used the SGLT tool (C++) in [8]. We set the location-removal probability par_c to 0.25, the location merging probability par_m to 0.75, and the randomization multiplication factor par_v to 4 in the same way as [9] (for details of the parameters in **SGLT**, see [9]). For the number c of semantic clusters, we attempted various values: $c = 50$, 100, 150, or 200 (as shown later, **SGLT** provided the best performance when $c = 50$ or 100). For each case, we set the probability par_l of removing the true location in the input training trace to various values from 0 to 1 ($par_l = 1$ in [9]) to evaluate the trade-off between the utility and privacy.

In **SGD** [10], we trained the transition matrix for each time slot ($|\mathcal{L}| \times |\mathcal{X}| \times |\mathcal{X}|$ elements in total) and the visit-probability vector for the first time instant ($|\mathcal{X}|$ elements in total) from the training traces via maximum likelihood estimation. Note that the transition matrix and the visit-probability vector are common to all users. Then we gener-

ated a synthetic trace from an input training trace by copying the first $\gamma \in \mathbb{Z}_{\geq 0}$ events and generating the remaining events using the trained transition matrix. When $\gamma = 0$, we randomly generated a location at the first time instant using the visit-probability vector. For more details of **SGD**, see Appendix D. We implemented **SGD** for location traces with C++, and made it public [1].

4.3 Performance Measures

Utility. We evaluated the utility listed in Section 1 as follows.

(a) *Time-dependent population distribution.* We first computed a frequency distribution ($|\mathcal{X}|$ -dimensional vector) of the testing traces and that of the synthetic traces for each time slot. Then we evaluated the average total variation between the two distributions over all time slots (denoted by **TP-TV**).

Note that frequently visited locations are especially important for some tasks [75, 19]. Thus for each time slot, we also selected the top 50 locations, whose frequencies in the testing traces were the largest, and regarded the absolute error for the remaining locations in **TP-TV** as 0 (**TP-TV-Top50**).

(b) *Transition matrix.* We computed an average transition-probability matrix ($|\mathcal{X}| \times |\mathcal{X}|$ matrix) over all users and all time instances from the testing traces. Similarly, we computed an average transition-probability matrix from the synthetic traces. Since each row of the transition-probability matrix represents a conditional distribution, we evaluated the EMD (Earth Mover’s Distance) between the two conditional distributions over the x -axis (longitude) and y -axis (latitude), and averaged it over all rows (**TM-EMD-X** and **TM-EMD-Y**). **TM-EMD-X** and **TM-EMD-Y** represent how the two transition matrices differ over the x -axis and y -axis, respectively.

(c) *Distribution of visit-fractions.* Since we used POIs in **FS** (regions in **PF**), we evaluated how well the synthetic traces preserve a distribution of visit-fractions in **FS**. We first excluded testing traces whose number of events are small (less than 5). Then, for each of the remaining traces, we computed a fraction of visits for each POI. Based on this, we computed a distribution of visit-fractions for each POI by dividing the fraction into 24 bins as follows: $(0, \frac{1}{24}]$, $(\frac{1}{24}, \frac{2}{24}]$, \dots , $(\frac{23}{24}, 1)$. Similarly, we computed a distribution of visit-fractions for each POI from the synthetic traces. Finally, we evaluated the EMD between the two distributions (**VF-EMD**).

(d) *Cluster-specific population distribution.* To show that **Proposal** is also effective in this aspect, we performed the following analysis. We utilized the fact that each column in the factor matrix **A** represents a cluster ($z = 16$ clusters in total). Specifically, for each column in **A**, we extracted the top 10% users whose values in the column are the largest. These users form a cluster who exhibit a similar behavior.

We computed, for each cluster, the frequency distribution of the training traces (averaged over all time slots), and that of the synthetic traces. Then we computed the maximum total variation between the two distributions over all clusters (**CP-TV**). Moreover, we visualized the distributions and factor matrices for some clusters.

Privacy. In **PF**, we evaluated the three synthesizers. Although **Proposal** and **SGD** provide (k, ϵ) -PD in Defini-

tion 2, **SGLT** are designed to provide PD using a semantic distance between traces [9], which is different from PD in Definition 2.

To compare the three synthesizers using the same privacy measure, we used the *re-identification rate* by the Bayesian adversary [45]. Specifically, we considered an adversary who identifies, for each synthetic trace, an *input user*, whose training trace is used to synthesize the trace, from $|\mathcal{U}|$ training users. We first trained the transition matrix for each training user from the training traces via maximum likelihood estimation. Then we re-identified each synthetic trace by selecting a training user whose posterior probability of being the input user is the highest (we computed the posterior probability by using the transition matrix and assuming a uniform prior; see [45] for details). We evaluated the re-identification rate as the proportion of synthetic traces correctly identified.

In **FS**, we used (k, ϵ) -PD in Definition 2 as a privacy measure, since we evaluated only **Proposal** and **SGD**. As a PD test, we used the (faster) **Privacy Test 1** with $|\mathcal{U}^*| = 32000$, $k = 10$, and $\epsilon = 1$, as described in Section 3.5.

Scalability. We measured the time to synthesize traces using the ABCI (AI Bridging Cloud Infrastructure) [49], which is a supercomputer ranking 8th in the Top 500 and 3rd in the Green 500 (as of June 2019). We used one computing node, which consists of two Intel Xeon Gold 6148 (27.5M Cache, 2.40 GHz, 20 Core) and 384GiB main memory.

4.4 Experimental Results in PF

Utility and privacy. Figure 7 shows the re-identification rate and utility with regard to (a) the time-dependent population distribution and (b) transition matrix in **PF**. Here, **Uniform** represents the utility when the uniform distribution is used as a distribution (i.e., the population distribution, each row of the transition matrix) of the synthetic traces. **Training** represents the utility of the training traces; i.e., the utility when we output the training traces as synthetic traces without modification. Ideally, the utility of the synthetic traces should be much better than that of **Uniform** and close to that of **Training**.

It can be seen from Figure 7 that **Proposal** achieves **TP-TV** and **TP-TV-Top50** close to **Training** for a small re-identification rate. For example, when the re-identification rate is required to be less than 0.02, **Proposal** achieves **TP-TV** = 0.43 and **TP-TV-Top50** = 0.13, both of which are close to those of **Training** (**TP-TV** = 0.39 and **TP-TV-Top50** = 0.12). In **SGLT** and **SGD**, the re-identification rate rapidly increases with decrease in **TP-TV** and **TP-TV-Top50**. This is because both **SGLT** and **SGD** synthesize traces by copying over some events from the training traces. Specifically, **SGLT** (resp. **SGD**) increases the number of copied events by decreasing par_l (resp. increasing γ). Although a larger number of copied events result in the decrease of both **TP-TV** and **TP-TV-Top50**, they also result in the rapid increase of the re-identification rate. This is consistent with the *uniqueness* of location data; e.g., only two (resp. three) locations are enough to uniquely characterize 50% (resp. 80%) of the individuals among one and a half million people [18].

It can also be seen that **Proposal** performs worse than **SGLT** and **SGD** with regard to **TM-EMD-X** and **TM-EMD-Y**. We consider this is because **Proposal** modifies the transition matrix so that it is consistent with a visit-

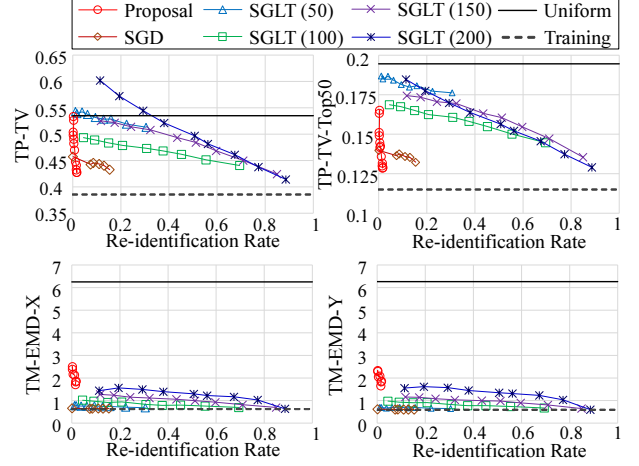


Figure 7: Re-identification rate and utility (**TP-TV**, **TP-TV-Top50**, **TM-EMD-X**, and **TM-EMD-Y**) in **PF**. The number in **SGLT** represents the number c of clusters.

Table 1: **CP-TV** in **PF** when the re-identification rate is required to be less than 0.02.

	Proposal	SGD	SGLT	Uniform
CP-TV	0.495	0.672	0.823	0.777

probability vector for each time slot using the MH algorithm (whereas **SGLT** and **SGD** do not modify the transition matrix). It should be noted, however, that **Proposal** significantly outperforms **Uniform** with regard to **TM-EMD-X** and **TM-EMD-Y**, which means that **Proposal** preserves the transition matrix well.

Next, we show the utility with regard to (d) the cluster-specific population distribution. Table 1 shows **CP-TV** when the re-identification rate is less than 0.02. It can be seen that **Proposal** achieves the lowest **CP-TV**. To explain the reason for this, we performed the following analysis.

Analysis on cluster-specific features. We visualize in Figure 8 the frequency distributions of training traces and synthetic traces and the columns of factor matrices **B** and **C** for three clusters (we set $\alpha = 200$, as it provided almost the best utility in Figure 7; we also normalized elements in each column of **B** and **C** so that the square-sum is one). Recall that for each cluster, we extracted the top 10% users; i.e., 50 users.

It can be seen that the frequency distributions of training traces are different from cluster to cluster, and the users in each cluster exhibit a similar behavior; e.g., the users in (i) stay in the northeastern area of Tokyo, whereas the users in (ii) and (iii) often use the subways. **Proposal** models such a cluster-specific behavior via **B** and **C**, and synthesizes traces that preserve the behavior using **B** and **C**. This explains the reason for a low value of **CP-TV** in **Proposal**. Figure 8 also shows that **Proposal** is useful for geo-data analysis such as modeling human location patterns [38] and map inference [39, 6].

Scalability. We also measured the time to synthesize traces from training traces. Here we generated one synthetic trace from each training trace (500 synthetic traces in total), and

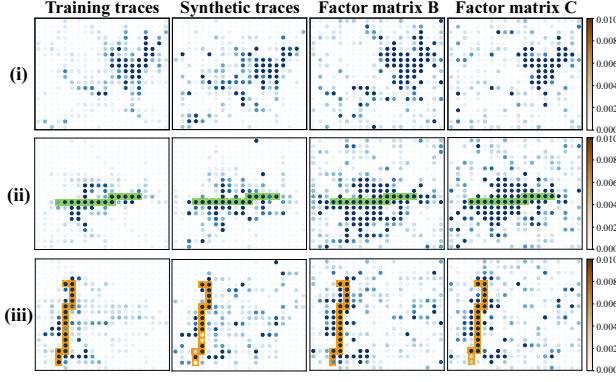


Figure 8: Frequency distributions and the columns of factor matrices B and C for three clusters (50 users for each cluster) in PF. The green line in (ii) and the orange line in (iii) represent subways (Shinjuku and Fukutoshin lines, respectively).

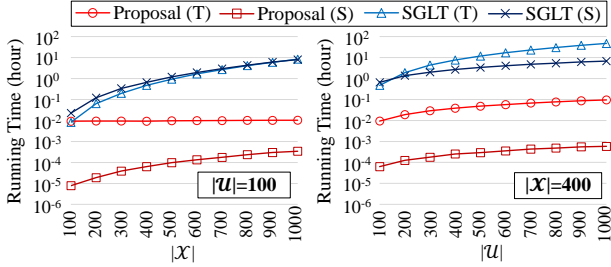


Figure 9: Running time in PF. “T” and “S” in the parentheses represent the time to train a generative model (i.e., MTF parameters in Proposal and semantic clusters in SGLT) and the time to generate 500 synthetic traces, respectively.

measured the time. We also changed the numbers of users and locations (i.e., $|\mathcal{U}|$, $|\mathcal{X}|$) for various values from 100 to 1000 to see how the running time depends on $|\mathcal{U}|$ and $|\mathcal{X}|$.

Figure 9 shows the results (we set $\alpha = 200$ in **Proposal**, and $c = 100$ and $par_l = 1$ in **SGLT**; we also obtained almost the same results for other values). Here we excluded the running time of **SGD**, since it was very small; e.g., less than one second when $|\mathcal{U}| = 1000$ and $|\mathcal{X}| = 400$ (we compare the running time of **Proposal** with that of **SGD** in **FS**, as shown later). It can be seen that the running time of **SGLT** is much larger than that of **Proposal**. Specifically, the running time of **SGLT** is quadratic in $|\mathcal{U}|$ (e.g., when $|\mathcal{X}| = 400$, **SGLT**(T) requires 0.47 and 47 hours for $|\mathcal{U}| = 100$ and 1000, respectively) and cubic in $|\mathcal{X}|$ (e.g., when $|\mathcal{U}| = 100$, **SGLT**(T) requires 8.1×10^{-3} and 8.4 hours for $|\mathcal{X}| = 100$ and 1000, respectively). On the other hand, the running time of **Proposal** is linear in $|\mathcal{U}|$ (e.g., **Proposal**(S) requires 6.3×10^{-5} and 5.9×10^{-4} hours for $|\mathcal{U}| = 100$ and 1000, respectively) and quadratic in $|\mathcal{X}|$ (e.g., **Proposal**(S) requires 9.3×10^{-3} and 0.96 hours for $|\mathcal{X}| = 100$ and 1000, respectively). This is consistent with the time complexity described in Section 3.1.

From Figure 9, we can also estimate the running time of **SGLT** for generating large-scale traces. Specifically, when $|\mathcal{U}| = 219793$ and $|\mathcal{X}| = 1000$ as in **IST** of **FS**, **SGLT**(T)

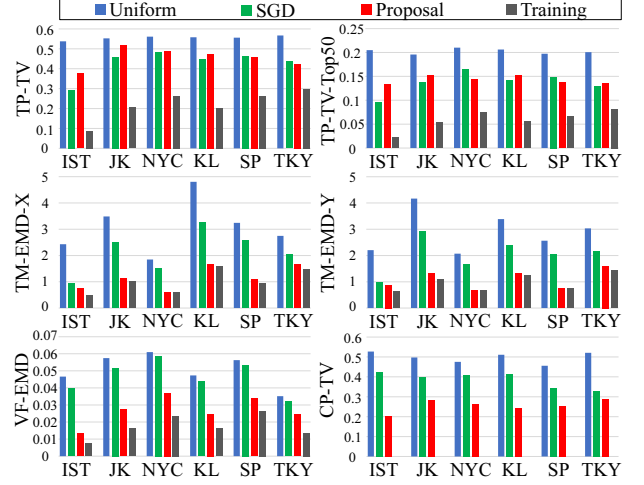


Figure 10: Utility of generated traces with (10,1)-PD in FS.

(semantic clustering) would require about 4632 years ($=8.4 \times (219793/100)^2 / (365 \times 24)$). Even if we use 1000 nodes of the ABCI (which has 1088 nodes [49]) in parallel, **SGLT**(T) would require over four years. Thus **SGLT** cannot be applied to **IST**, and hence we compare **Proposal** with **SGD** in **FS**.

4.5 Experimental Results in FS

Utility and privacy. In **FS**, we used (k, ϵ) -PD as a privacy measure, and set $k = 10$ and $\epsilon = 1$. We confirmed that about 60% to 70% of the synthetic traces passed the PD-test, and the utility was hardly affected by introducing the PD-test (see Appendix F for details). In **Proposal**, we set $\alpha = 200$ (as in Figures 8 and 9). In **SGD**, we set $\gamma = 0$ for the following two reasons: (1) the re-identification rate is high for $\gamma \geq 1$ in Figure 7 due to the *uniqueness* of location data [18]; (2) the event in the first time slot is missing for many users in **FS**, and cannot be copied. Note that **SGD** with $\gamma = 0$ always passes the PD test, since it generates synthetic traces independently of the input data record [10]. We evaluated all of the utility measures for **Proposal** and **SGD**.

Figure 10 shows that for **TP-TV** and **TP-TV-Top50**, **Proposal** performs worse than **SGD** in **IST** and **JK**, but as well as **SGD** in the other cities. This is because **SGD** uses the transition matrix common to all users, and the number of elements in the transition matrix does not depend on $|\mathcal{U}|$. Consequently, **SGD** can preserve the time-dependent population distribution effectively, especially when $|\mathcal{U}|$ is large (as in **IST** and **JK**).

However, for **TM-EMD-X** and **TM-EMD-Y**, **Proposal** outperforms **SGD**, especially in **JK**, **NYC**, **KL**, and **SP**. This is because there are many missing events in **FS**, and the number of transitions in the training traces is small in **JK**, **NYC**, **KL**, and **SP** (as described in Section 4.1). Note that the population distribution consists of $|\mathcal{X}|$ values, whereas the transition matrix consists of $|\mathcal{X}| \times |\mathcal{X}|$ values. Since the number of latter values is much larger, it is much harder to accurately estimate the transition matrix itself.

A crucial difference between **Proposal** and **SGD** lies at the fact that **Proposal** models the user/cluster-specific mo-

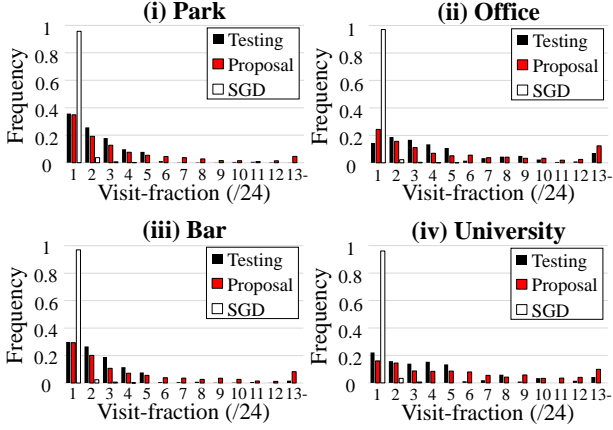


Figure 11: Distributions of visit-fractions for four POI categories (park, office, bar, and university) in NYC.

bility features, while **SGD** ($\gamma = 0$) does not. This causes the results of **TF-EMD** and **CP-TV** in Figure 10. Specifically, for **TF-EMD**, **SGD** performs almost the same as **Uniform**, whereas **Proposal** significantly outperforms **SGD**. For **CP-TV**, **Proposal** also significantly outperforms **SGD**. To explain this in more detail, we performed the following analysis.

Analysis on user/cluster-specific features. First, we show in Figure 11 the distributions of visit-fractions for four POI categories in NYC (**Testing** represents the distribution of testing traces). It can be seen that the distribution of **SGD** concentrates at the visit-fraction of 1/24 (i.e., 0 to 0.042). This is because **SGD** ($\gamma = 0$) uses the transition matrix and visit-probability vector common to all users, and synthesizes traces independently of input training traces. Consequently, all users spend almost the same amount of time on each POI category. On the other hand, **Proposal** models the user-specific mobility feature via two tensors, and generates traces based on the mobility feature of the input training trace. As a result, the distribution of **Proposal** is similar to that of **Testing**, and reflects the fact that about 30 to 35% of users spend less than 1/24 of their time at park or bar, whereas about 80% of users spend more than 1/24 of their time at office or university. This explains the low values of **TF-EMD** in **Proposal**. Figure 11 also shows that the distributions in **Proposal** are useful for semantic annotation of POIs [19, 71].

Next, we visualize in Figure 12 the columns of factor matrices **B** and **D** and training/synthetic traces for two clusters. As with **PF**, the training users in each cluster exhibit a similar behavior; e.g., the users in (i) enjoy great outdoors and shopping at mall, whereas the users in (ii) go to universities. Note that users and POIs in each cluster are *semantically* similar; e.g., people who enjoy great outdoors also enjoy shopping at mall; many users in (ii) would be students, faculty, or staff. The activity time is also different between the two clusters. For example, we confirmed that many training users in (i) enjoy great outdoors and shopping from morning until night, whereas most training users in (ii) are not in the universities at night. **Proposal**

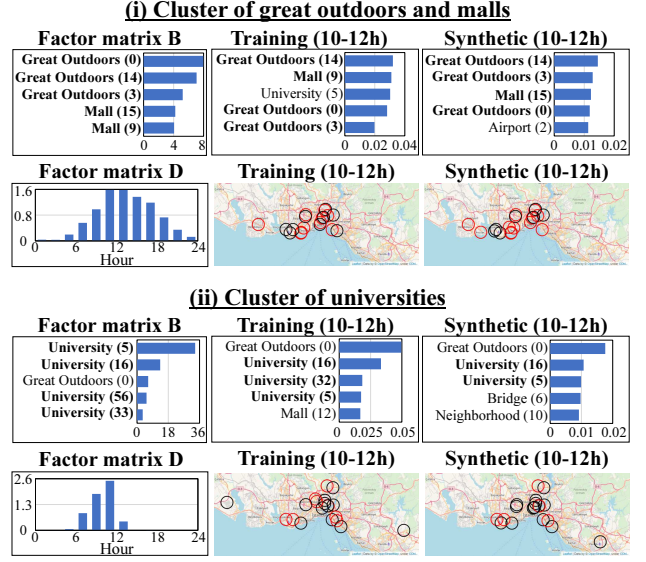


Figure 12: Two clusters in IST (21980 users for each cluster). For **B** and training/synthetic traces, we show the top 5 POIs (numbers in the parentheses represent POI IDs), whose values or frequencies from 10:00 to 12:00 are the highest. We also show the top 20 POIs in the map by circles. Red circles in (i) (resp. (ii)) represent outdoors/malls (resp. universities).

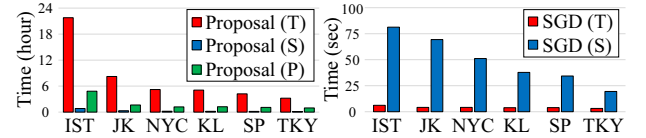


Figure 13: Running time in FS. “T”, “S”, and “P” represent the time to train a generative model, the time to synthesize traces, and the time to run the PD test, respectively.

models such a behavior via factor matrices, and synthesizes traces preserving the behavior. This explains the low values of **CP-TV** in **Proposal**. We emphasize that this aspect is useful for various geo-data analysis; e.g., modeling human location patterns, semantic annotation of POIs.

Note that some utility values of both **Proposal** and **SGD** might be improved by estimating missing events in training traces [60, 44]. However, **TF-EMD** and **CP-TV** of **SGD** ($\gamma = 0$) cannot be improved even by estimating missing events, as it does not model the user/cluster-specific features.

Scalability. We measured the running time in FS. Figure 13 shows that **SGD** is much faster than **Proposal**; e.g., in **IST**, **Proposal** requires about one day to synthesize traces, whereas **SGD** requires less than two minutes. The reason for this lies in the simplicity of **SGD**; i.e., **SGD** trains a transition matrix for each time slot via maximum likelihood estimation, and then synthesizes traces using the transition matrix. However, **SGD** ($\gamma = 0$) does not gen-

erate user/cluster-specific traces. To generate such traces, **Proposal** is necessary.

5. CONCLUSION

In this paper, we propose a novel location synthesizer called PPMTF to make large-scale traces generation practical. We comprehensively showed that the proposed method provides high utility with regard to various geo-data analysis ((a)-(d)), high privacy, and high scalability.

6. ADDITIONAL AUTHORS

7. REFERENCES

- [1] Tool: Privacy-preserving multiple tensor factorization (PPMTF). <https://github.com/PPMTF/PPMTF>.
- [2] PWS Cup 2019. https://www.iwsec.org/pws/2019/cup19_e.html, 2019.
- [3] C. C. Aggarwal. *Recommender Systems*. Springer, 2016.
- [4] R. Albright, J. Cox, D. Duling, A. N. Langville, and C. D. Meyer. Algorithms, initializations, and convergence for the nonnegative matrix factorization. *SAS Technical Report*, pages 1–18, 2014.
- [5] M. E. Andrés, N. E. Bordenabe, K. Chatzikokolakis, and C. Palamidessi. Geo-indistinguishability: Differential privacy for location-based systems. In *Proceedings of the 20th ACM Conference on Computer and Communications Security (CCS'13)*, pages 901–914, 2013.
- [6] J. Biagioni and J. Eriksson. Inferring road maps from global positioning system traces: Survey and comparative evaluation. *Journal of the Transportation Research Board*, 2291(2291):61–71, 2012.
- [7] I. Bilogrevic, K. Huguenin, M. Jadliwala, F. Lopez, J.-P. Hubaux, P. Ginzboorg, and V. Niemi. Inferring social ties in academic networks using short-range wireless communications. In *Proceedings of the 12th ACM Workshop on Privacy in the Electronic Society (WPES'13)*, pages 179–188, 2013.
- [8] V. Bindschaedler and R. Shokri. Synthetic location traces generator (sglt). <https://vbinds.ch/node/70>.
- [9] V. Bindschaedler and R. Shokri. Synthesizing plausible privacy-preserving location traces. In *Proceedings of the 2016 IEEE Symposium on Security and Privacy (S&P'16)*, pages 546–563, 2016.
- [10] V. Bindschaedler, R. Shokri, and C. A. Gunter. Plausible deniability for privacy-preserving data synthesis. *Proceedings of the VLDB Endowment*, 10(5):481–492, 2017.
- [11] C. Bishop. *Pattern Recognition and Machine Learning*. Springer, 2006.
- [12] K. Chatzikokolakis, E. Elsalamouny, C. Palamidessi, and A. Pazii. Methods for location privacy: A comparative overview. *Foundations and Trends in Privacy and Security*, 1(4):199–257, 2017.
- [13] E. Cho, S. A. Myers, and J. Leskovec. Friendship and mobility: User movement in location-based social networks. In *Proceedings of the 17th ACM SIGKDD International Conference on Knowledge Discovery and Data Mining (KDD'11)*, pages 1082–1090, 2011.
- [14] C.-Y. Chow and M. F. Mokbel. Trajectory privacy in location-based services and data publication. *ACM SIGKDD Explorations Newsletter*, 13(1):19–29, 2011.
- [15] R. Chow and P. Golle. Faking contextual data for fun, profit, and privacy. In *Proceedings of the 8th ACM Workshop on Privacy in the Electronic Society (WPES'09)*, pages 105–108, 2009.
- [16] A. Cichocki, R. Zdunek, A. H. Phan, and S. Amari. *Nonnegative Matrix and Tensor Factorizations: Applications to Exploratory Multi-way Data Analysis and Blind Source Separation*. Wiley, 2009.
- [17] J. Cranshaw, R. Schwartz, J. I. Hong, and N. Sadeh. The livelihoods project: Utilizing social media to understand the dynamics of a city. In *Proceedings of the Sixth International AAAI Conference on Weblogs and Social Media (ICWSM'12)*, pages 58–65, 2012.
- [18] Y.-A. de Montjoye, C. A. Hidalgo, M. Verleysen, and V. D. Blondel. Unique in the crowd: The privacy bounds of human mobility. *Scientific Reports*, 3(1376):1–5, 2013.
- [19] T. M. T. Do and D. Gatica-Perez. The places of our lives: Visiting patterns and automatic labeling from longitudinal smartphone data. *IEEE Transactions on Mobile Computing*, 13(3):638–648, 2013.
- [20] C. Dwork. Differential privacy. In *Proceedings of the 33rd international conference on Automata, Languages and Programming (ICALP'06)*, pages 1–12, 2006.
- [21] C. Dwork and A. Roth. *The Algorithmic Foundations of Differential Privacy*. Now Publishers, 2014.
- [22] C. Dwork and A. Smith. Differential privacy for statistics: What we know and what we want to learn. *Journal of Privacy and Confidentiality*, 1(2):135–154, 2009.
- [23] N. Eagle, A. Pentland, and D. Lazer. Inferring friendship network structure by using mobile phone data. *Proceedings of the National Academy of Sciences (PNAS)*, 106(36):15274–15278, 2009.
- [24] J. Ernvall and O. Nevalainen. An algorithm for unbiased random sampling. *The Computer Journal*, 25(1):45–47, 1982.
- [25] B. Gedik and L. Liu. Protecting location privacy with personalized k-anonymity: Architecture and algorithms. *IEEE Transactions on Mobile Computing*, 7(1):1–18, 2008.
- [26] G. Ghinita. *Privacy for Location-based Services*. Morgan & Claypool Publishers, 2013.
- [27] M. Herrmann, C. Troncoso, C. Diaz, and B. Preneel. Optimal sporadic location privacy preserving systems in presence of bandwidth constraints. In *Proceedings of the 12th ACM Workshop on Privacy in the Electronic Society (WPES'13)*, pages 167–178, 2013.
- [28] B. Hoh, M. Gruteser, H. Xiong, and A. Alrabady. Achieving guaranteed anonymity in GPS traces via uncertainty-aware path cloaking. *IEEE Transactions on Mobile Computing*, 9(8):1089–1107, 2010.
- [29] H. Hu, J. Xu, Q. Chen, and Z. Yang. Authenticating location-based services without compromising location privacy. In *Proceedings of the 2012 ACM SIGMOD International Conference on Management of Data (SIGMOD'12)*, pages 301–312, 2012.
- [30] Y. Hu, Y. Koren, and C. Volinsky. Collaborative

- filtering for implicit feedback datasets. In *Proceedings of the 8th IEEE International Conference on Data Mining (ICDM'08)*, pages 263–272, 2008.
- [31] R. Kato, M. Iwata, T. Hara, A. Suzuki, X. Xie, Y. Arase, and S. Nishio. A dummy-based anonymization method based on user trajectory with pauses. In *Proceedings of the 20th International Conference on Advances in Geographic Information Systems (SIGSPATIAL'12)*, pages 249–258, 2012.
- [32] Y. Kawamoto and T. Murakami. Local obfuscation mechanisms for hiding probability distributions. In *Computer Security - ESORICS 2019 - 24th European Symposium on Research in Computer Security, Luxembourg, September 23-27, 2019, Proceedings, Part I*, pages 128–148, 2019.
- [33] R. H. Keshavan, A. Montanari, and S. Oh. Matrix completion from noisy entries. In *Proceedings of the 22nd Conference on Neural Information Processing Systems (NIPS'09)*, pages 952–960, 2009.
- [34] S. A. Khan and S. Kaski. Bayesian multi-view tensor factorization. In *Proceeding of the European Conference on Machine Learning and Principles and Practice of Knowledge Discovery in Databases (ECML PKDD'14)*, pages 656–671, 2014.
- [35] H. Kido, Y. Yanagisawa, and T. Satoh. An anonymous communication technique using dummies for location-based services. *Proceedings of the 2005 IEEE International Conference on Pervasive Services (ICPS'05)*, pages 88–97, 2005.
- [36] J. Krumm. A survey of computational location privacy. *Personal and Ubiquitous Computing*, 13(6):391–399, 2009.
- [37] N. Li, M. Lyu, and D. Su. *Differential Privacy: From Theory to Practice*. Morgan & Claypool Publishers, 2016.
- [38] M. Lichman and P. Smyth. Modeling human location data with mixtures of kernel densities. In *Proceedings of the 20th ACM SIGKDD International Conference on Knowledge Discovery and Data Mining (KDD'14)*, pages 35–44, 2014.
- [39] X. Liu, J. Biagioni, J. Eriksson, Y. Wang, G. Forman, and Y. Zhu. Mining large-scale, sparse gps traces for map inference: Comparison of approaches. In *Proceedings of the 18th ACM SIGKDD international conference on Knowledge discovery and data mining (KDD'12)*, pages 669–677, 2012.
- [40] X. Liu, Y. Liu, K. Aberer, and C. Miao. Personalized point-of-interest recommendation by mining users' preference transition. In *Proceedings of the 22nd ACM international conference on Information & Knowledge Management (CIKM'13)*, pages 733–738, 2013.
- [41] Z. Liu, Y.-X. Wang, and A. J. Smola. Fast differentially private matrix factorization. In *Proceedings of the 9th ACM Conference on Recommender Systems (RecSys'15)*, pages 171–178, 2015.
- [42] A. Machanavajjhala, J. Gehrke, D. Kifer, and M. Venkitasubramaniam. l-diversity: Privacy beyond k-anonymity. In *Proceedings of the 22nd International Conference on Data Engineering (ICDE'06)*, pages 24–35, 2006.
- [43] Y. Matsuo, N. Okazaki, K. Izumi, Y. Nakamura, T. Nishimura, and K. Hasida. Inferring long-term user properties based on users' location history. In *Proceedings of the 20th International Joint Conference on Artificial Intelligence (IJCAI'07)*, pages 2159–2165, 2007.
- [44] T. Murakami. Expectation-maximization tensor factorization for practical location privacy attacks. *Proceedings on Privacy Enhancing Technologies (PoPETs)*, 4:138–155, 2017.
- [45] T. Murakami, A. Kanemura, and H. Hino. Group sparsity tensor factorization for de-anonymization of mobility traces. In *Proceedings of the 14th IEEE International Conference on Trust, Security and Privacy in Computing and Communications (TrustCom'15)*, pages 621–629, 2015.
- [46] T. Murakami and Y. Kawamoto. Utility-optimized local differential privacy mechanisms for distribution estimation. In *Proceedings of the 28th USENIX Security Symposium (USENIX'19)*, pages 1877–1894, 2019.
- [47] T. Murakami and H. Watanabe. Localization attacks using matrix and tensor factorization. *IEEE Transactions on Information Forensics and Security*, 11(8):1647–1660, 2016.
- [48] K. P. Murphy. *Machine Learning: A Probabilistic Perspective*. The MIT Press, 2012.
- [49] National Institute of Advanced Industrial Science and Technology (AIST). AI bridging cloud infrastructure (ABCI). <https://abci.ai/>.
- [50] Nightley and Center for Spatial Information Science at the University of Tokyo (CSIS). SNS-based people flow data. <http://nightley.jp/archives/1954>, 2014.
- [51] R. Pan, Y. Zhou, B. Cao, N. N. Liu, R. Lukose, M. Scholz, and Q. Yang. One-class collaborative filtering. In *Proceedings of the 8th IEEE International Conference on Data Mining (ICDM'08)*, pages 502–511, 2008.
- [52] K. B. Petersen and M. S. Pedersen. The matrix cookbook. <http://matrixcookbook.com>, 2012.
- [53] M. Piorkowski, N. Sarafijanovic-Djukic, and M. Grossglauser. CRAWDAD dataset epfl/mobility (v. 2009-02-24). <http://crawdad.org/epfl/mobility/20090224>, 2009.
- [54] Please Rob Me - Raising Awareness about Over-sharing. <http://pleaseroame.com/>, 2010.
- [55] V. Primault, A. Boutet, S. B. Mokhtar, and L. Brunie. The long road to computational location privacy: A survey. *IEEE Communications Surveys & Tutorials*, 21(3):2772–2793, 2019.
- [56] R. Salakhutdinov and A. Mnih. Probabilistic matrix factorization. In *Proceedings of the 20th International Conference on Neural Information Processing Systems (NIPS'07)*, pages 1257–1264, 2007.
- [57] R. Salakhutdinov and A. Mnih. Bayesian probabilistic matrix factorization using markov chain monte carlo. In *Proceedings of the 25th International Conference on Machine Learning (ICML'08)*, pages 880–887, 2008.
- [58] Y. Sekimoto, R. Shibasaki, H. Kanasugi, T. Usui, and Y. Shimazaki. PFlow: Reconstructing people flow recycling large-scale social survey data. *IEEE Pervasive Computing*, 10(4):27–35, 2011.

[59] S. Shekhar, M. R. Evans, V. Gunturi, and K. Yang. Spatial big-data challenges intersecting mobility and cloud computing. In *Proceedings of the 11th ACM International Workshop on Data Engineering for Wireless and Mobile Access (MobiDE'12)*, pages 1–12, 2012.

[60] R. Shokri, G. Theodorakopoulos, J.-Y. L. Boudec, and J.-P. Hubaux. Quantifying location privacy. In *Proceedings of the 2011 IEEE Symposium on Security and Privacy (S&P'11)*, pages 247–262, 2011.

[61] R. Shokri, G. Theodorakopoulos, G. Danezis, J.-P. Hubaux, and J.-Y. L. Boudec. Quantifying location privacy: The case of sporadic location exposure. In *Proceedings of the 11th International Conference on Privacy Enhancing Technologies (PETS'11)*, pages 57–76, 2011.

[62] R. Shokri, G. Theodorakopoulos, C. Troncoso, J.-P. Hubaux, and J.-Y. L. Boudec. Protecting location privacy: Optimal strategy against localization attacks. *Proceedings of the 2012 ACM Conference on Computer and Communications Security (CCS'12)*, pages 617–627, 2012.

[63] L. Song, D. Kotz, R. Jain, and X. He. Evaluating next-cell predictors with extensive wi-fi mobility data. *IEEE Transactions on Mobile Computing*, 5(12):1633–1649, 2006.

[64] A. Suzuki, M. Iwata, Y. Arase, T. Hara, X. Xie, and S. Nishio. A user location anonymization method for location based services in a real environment. In *Proceedings of the 18th SIGSPATIAL International Conference on Advances in Geographic Information Systems (GIS'10)*, pages 398–401, 2010.

[65] K. Takeuchi, R. Tomioka, K. Ishiguro, A. Kimura, and H. Sawada. Non-negative multiple tensor factorization. In *Proceedings of the IEEE 13th International Conference on Data Mining (ICDM'13)*, pages 1199–1204, 2013.

[66] J. Voelcker. Stalked by satellite: An alarming rise in GPS-enabled harassment. *IEEE Spectrum*, 47(7):15–16, 2006.

[67] Y.-X. Wang, S. E. Fienberg, and A. J. Smola. Privacy for free: Posterior sampling and stochastic gradient monte carlo. In *Proceedings of the 32nd International Conference on International Conference on Machine Learning (ICML'15)*, pages 2493–2502, 2015.

[68] A. Y. Xue, R. Zhang, Y. Zheng, X. Xie, J. Huang, and Z. Xu. Destination prediction by sub-trajectory synthesis and privacy protection against such prediction. In *Proceedings of the 2013 IEEE International Conference on Data Engineering (ICDE'13)*, pages 254–265, 2013.

[69] D. Yang, B. Qu, J. Yang, and P. Cudre-Mauroux. Revisiting user mobility and social relationships in LBSNs: A hypergraph embedding approach. In *Proceedings of the 2019 World Wide Web Conference (WWW'19)*, pages 2147–2157, 2019.

[70] D. Yang, D. Zhang, and B. Qu. Participatory cultural mapping based on collective behavior data in location based social network. *ACM Transactions on Intelligent Systems and Technology*, 7(3):30:1–30:23, 2016.

[71] M. Ye, D. Shou, W.-C. Lee, P. Yin, and K. Janowicz. On the semantic annotation of places in

location-based social networks. In *Proceedings of the 17th ACM SIGKDD International Conference on Knowledge Discovery and Data Mining (KDD'11)*, pages 520–528, 2011.

[72] T.-H. You, W.-C. Peng, and W.-C. Lee. Protecting moving trajectories with dummies. In *Proceedings of the 2007 International Conference on Mobile Data Management (MDM'07)*, pages 278–282, 2007.

[73] V. W. Zheng, Y. Zheng, and Q. Yang. Joint learning user's activities and profiles from GPS data. In *Proceedings of the 2009 International Workshop on Location Based Social Networks (LBSN'09)*, pages 17–20, 2009.

[74] Y. Zheng, X. Xie, and W.-Y. Ma. GeoLife: A collaborative social networking service among user, location and trajectory. *IEEE Data Engineering Bulletin*, 32(2):32–40, 2010.

[75] Y. Zheng, L. Zhang, X. Xie, and W.-Y. Ma. Mining interesting locations and travel sequences from GPS trajectories. In *Proceedings of the 18th International Conference on World Wide Web (WWW'09)*, pages 791–800, 2009.

APPENDIX

A. NOTATIONS

We show the basic notations used in this paper in Table 2.

B. TIME COMPLEXITY

Now we describe the time complexity of the proposed method described in Section 3 in detail. We assume that we generate a synthetic trace from each training trace $s_n \in \mathcal{S}$ (i.e., $|\mathcal{U}|$ synthetic traces in total) and perform the PD test for each synthetic trace. We also assume that $\lambda^I, \rho^I, \lambda^{II}, \rho^{II}, z$, and $|\mathcal{U}^*|$ are constants (note that typically $\lambda^I, \rho^I \ll |\mathcal{X}| \times |\mathcal{X}'|$, $\lambda^{II}, \rho^{II} \ll |\mathcal{X}| \times |\mathcal{L}|$, and $z \ll \min(|\mathcal{U}|, |\mathcal{X}'|)$, as described in Sections 3.2 and 3.3; a small value of $|\mathcal{U}^*|$ is also used for fast PD test, as described in Section 3.5).

In the step (i), we simply count the number of transitions and the number of visits from a training trace set \mathcal{S} . Thus, the computation time of this step is very small, compared to that of the remaining four steps.

In the step (ii), we first randomly sample ρ^I and ρ^{II} zero elements for each user in \mathbf{R}^I and \mathbf{R}^{II} , respectively. This can be done in $O(|\mathcal{U}|)$ time in total by using a sampling technique in [24]. Subsequently, we train the MTF parameters Θ via the Gibbs sampling. The computation time of the Gibbs sampling can be expressed as $O(|\mathcal{U}| + |\mathcal{X}| + |\mathcal{L}|)$.

In the steps (iii) and (iv), we generate synthetic traces via the MH algorithm. The step (iii) is dominated by computing the transition-probability matrices $\mathbf{Q}_n^*, \mathbf{Q}_{n,1}, \dots, \mathbf{Q}_{n,|\mathcal{L}|}$ for each training trace s_n , which takes $O(|\mathcal{U}||\mathcal{X}'|^2|\mathcal{L}|)$ time in total. The step (iv) requires $O(|\mathcal{U}||\mathcal{X}'||\mathcal{L}|)$ time.

In the step (v), assume that we use the faster version of **Privacy Test 1** (described in Section 3.5). Then we compute the transition-probability matrices $\mathbf{Q}_m^*, \mathbf{Q}_{m,1}, \dots, \mathbf{Q}_{m,|\mathcal{L}|}$ for each training trace $s_m \in \mathcal{S}^*$, which takes $O(|\mathcal{X}'|^2|\mathcal{L}|)$ time. Subsequently, we check whether $k' \geq k$ for each training trace $s_n \in \mathcal{S}$, which takes $O(|\mathcal{U}||\mathcal{X}'||\mathcal{L}|)$ time.

In summary, the time complexity of the proposed method can be expressed as $O(|\mathcal{U}||\mathcal{X}'|^2|\mathcal{L}|)$.

Table 2: Basic notations in this paper (\dagger represents I or II). The notations in the first and second groups are introduced in Sections 2 and 3, respectively.

Symbol	Description
\mathcal{U}	Finite set of training users.
\mathcal{X}	Finite set of locations.
\mathcal{T}	Finite set of time instants over \mathbb{N} .
\mathcal{L}	Finite set of time slots ($\mathcal{L} \subseteq \mathcal{P}(\mathcal{T})$).
\mathcal{E}	Finite set of events ($\mathcal{E} = \mathcal{X} \times \mathcal{T}$).
\mathcal{R}	Finite set of traces ($\mathcal{R} = \mathcal{U} \times \mathcal{E}^*$).
\mathcal{S}	Finite set of training traces ($\mathcal{S} \subseteq \mathcal{R}$).
\mathcal{F}	Randomized algorithm with domain $\mathcal{P}(\mathcal{R})$.
\mathcal{M}	Generative model.
u_n	n -th training user ($u_n \in \mathcal{U}$).
x_i	i -th location ($x_i \in \mathcal{X}$).
s_n	n -th training trace ($s_n \in \mathcal{S}$).
y	Synthetic trace ($y \in \mathcal{R}$).
\mathbf{R}^I	Transition-count tensor ($\mathbf{R}^I \in \mathbb{Z}_{\geq 0}^{ \mathcal{U} \times \mathcal{X} \times \mathcal{X} }$).
\mathbf{R}^{II}	Visit-count tensor ($\mathbf{R}^{II} \in \mathbb{Z}_{\geq 0}^{ \mathcal{U} \times \mathcal{X} \times \mathcal{L} }$).
\mathbf{R}	Tuple of two tensors ($\mathbf{R} = (\mathbf{R}^I, \mathbf{R}^{II})$).
$\hat{\mathbf{R}}^\dagger$	Approximation of \mathbf{R}^\dagger (reconstructed value).
$r_{n,i,j}^\dagger$	(n, i, j) -th element of \mathbf{R}^\dagger .
$\hat{r}_{n,i,j}^\dagger$	Approximation of $r_{n,i,j}^\dagger$ (reconstructed value).
\mathbf{A}	Factor matrix in the “User” mode.
\mathbf{B}	Factor matrix in the “Location” mode.
\mathbf{C}	Factor matrix in the “Next Location” mode.
\mathbf{D}	Factor matrix in the “Time Slot” mode.
Θ	Tuple of MTF parameters ($\Theta = (\mathbf{A}, \mathbf{B}, \mathbf{C}, \mathbf{D})$).
z	Number of columns in each factor matrix.
\mathcal{Q}	Set of transition-probability matrices.
\mathcal{C}	Set of visit-probability vectors.
\mathcal{F}_{PPMTF}	Proposed training algorithm.
\mathcal{M}_{PPMTF}	Proposed generative model.
$\mathbf{Q}_{n,i}$	Transition-probability matrix of user u_n for time slot l_i in \mathcal{M}_{PPMTF} ($\mathbf{Q}_{n,i} \in \mathcal{Q}$).
$\pi_{n,i}$	Visit-probability vector of user u_n for time slot l_i in \mathcal{M}_{PPMTF} ($\pi_{n,i} \in \mathcal{C}$).
λ^\dagger	Maximum number of positive elements per user in \mathbf{R}^\dagger .
ρ^\dagger	Number of sampled zero elements per user in \mathbf{R}^\dagger .
r_{max}^\dagger	Maximum value of counts for each element in \mathbf{R}^\dagger .
$I_{n,i,j}^\dagger$	Indicator function that takes 0 if $r_{n,i,j}^\dagger$ is missing, and takes 1 otherwise.

C. PROOF OF PROPOSITION 1

Let $\varepsilon \in \mathbb{R}_{\geq 0}$ be the value given by

$$\varepsilon = \alpha((\lambda^I + \rho^I)(r_{max}^I + \kappa)^2 + (\lambda^{II} + \rho^{II})(r_{max}^{II} + \kappa)^2). \quad (9)$$

By (4), the logarithm of $p(\Theta|\mathbf{R})$ can be written as follows:

$$\begin{aligned} & \ln p(\Theta|\mathbf{R}) \\ &= \ln p(\mathbf{R}|\Theta) + \ln p(\Theta) - \ln p(\mathbf{R}) \quad (\text{by Bayes' theorem}) \\ &= \sum_{n=1}^{|\mathcal{U}|} \sum_{i=1}^{|\mathcal{X}|} \sum_{j=1}^{|\mathcal{X}|} I_{n,i,j}^I \ln \mathcal{N}(r_{n,i,j}^I | \hat{r}_{n,i,j}^I, \alpha^{-1}) \\ & \quad + \sum_{n=1}^{|\mathcal{U}|} \sum_{i=1}^{|\mathcal{X}|} \sum_{j=1}^{|\mathcal{L}|} I_{n,i,j}^{II} \ln \mathcal{N}(r_{n,i,j}^{II} | \hat{r}_{n,i,j}^{II}, \alpha^{-1}) \\ & \quad + \ln p(\Theta) - \ln p(\mathbf{R}) \quad (\text{by (4)}) \\ &= - \sum_{n=1}^{|\mathcal{U}|} \sum_{i=1}^{|\mathcal{X}|} \sum_{j=1}^{|\mathcal{X}|} I_{n,i,j}^I \left(\frac{(\alpha(r_{n,i,j}^I - \hat{r}_{n,i,j}^I)^2)}{2} + \ln \sqrt{\frac{\alpha}{2\pi}} \right) \\ & \quad - \sum_{n=1}^{|\mathcal{U}|} \sum_{i=1}^{|\mathcal{X}|} \sum_{j=1}^{|\mathcal{L}|} I_{n,i,j}^{II} \left(\frac{(\alpha(r_{n,i,j}^{II} - \hat{r}_{n,i,j}^{II})^2)}{2} + \ln \sqrt{\frac{\alpha}{2\pi}} \right) \\ & \quad + \ln p(\Theta) - \ln p(\mathbf{R}). \end{aligned} \quad (10)$$

Let G be a function that takes as input two tensors \mathbf{R} and the MTF parameters Θ and outputs $G(\mathbf{R}, \Theta) \in \mathbb{R}$ as follows:

$$\begin{aligned} G(\mathbf{R}, \Theta) &= \sum_{n=1}^{|\mathcal{U}|} \sum_{i=1}^{|\mathcal{X}|} \sum_{j=1}^{|\mathcal{X}|} \frac{\alpha I_{n,i,j}^I (r_{n,i,j}^I - \hat{r}_{n,i,j}^I)^2}{2} \\ & \quad + \sum_{n=1}^{|\mathcal{U}|} \sum_{i=1}^{|\mathcal{X}|} \sum_{j=1}^{|\mathcal{L}|} \frac{\alpha I_{n,i,j}^{II} (r_{n,i,j}^{II} - \hat{r}_{n,i,j}^{II})^2}{2} \\ & \quad - \ln p(\Theta). \end{aligned} \quad (11)$$

Note that $\ln \sqrt{\frac{\alpha}{2\pi}}$ and $\ln p(\mathbf{R})$ in (10) do not depend on Θ . Thus, by (11), $\ln p(\Theta|\mathbf{R})$ in (10) can be expressed as follows:

$$p(\Theta|\mathbf{R}) = \frac{\exp[-G(\mathbf{R}, \Theta)]}{\int_{\Theta} \exp[-G(\mathbf{R}, \Theta)] d\Theta}. \quad (12)$$

Then, Proposition 1 can be proved by using the fact that \mathcal{F}_{PPMTF} is the exponential mechanism [21] that uses $-G(\mathbf{R}, \Theta)$ as a utility function. Specifically, let \mathbf{R}' be the tuple of two tensors that differ from \mathbf{R} at most one user's elements; i.e., \mathbf{R} and \mathbf{R}' are *neighboring*. We write $\mathbf{R} \sim \mathbf{R}'$ to represent that \mathbf{R} and \mathbf{R}' are neighboring. Let $\Delta G \in \mathbb{R}$ be the sensitivity of G given by:

$$\Delta G = \max_{\Theta} \max_{\mathbf{R}, \mathbf{R}' : \mathbf{R} \sim \mathbf{R}'} |G(\mathbf{R}, \Theta) - G(\mathbf{R}', \Theta)|. \quad (13)$$

Note that in (11), $I_{n,i,j}^I$ (resp. $I_{n,i,j}^{II}$) takes 1 at most $\lambda^I + \rho^I$ (resp. $\lambda^{II} + \rho^{II}$) elements for each user, as described in Section 3.3. In addition, $r_{n,i,j}^I \in [0, r_{max}^I]$, $r_{n,i,j}^{II} \in [0, r_{max}^{II}]$, $\hat{r}_{n,i,j}^I \in [-\kappa, r_{max}^I + \kappa]$, and $\hat{r}_{n,i,j}^{II} \in [-\kappa, r_{max}^{II} + \kappa]$ for each n, i, j , as described in Section 3.5. Thus, by (9), the sum of the first and second terms in (11) is less than (resp. more than) or equal to $\frac{\varepsilon}{2}$ in (resp. 0). Then, since the third term in (11) is the same for $G(\mathbf{R}, \Theta)$ and $G(\mathbf{R}', \Theta)$ in (13), ΔG can be bounded above by $\frac{\varepsilon}{2}$: i.e., $\Delta G \leq \frac{\varepsilon}{2}$.

Finally, we show that the ratio between $p(\Theta = \mathcal{F}_{PPMTF}(\mathbf{R}))$ and $p(\Theta = \mathcal{F}_{PPMTF}(\mathbf{R}'))$ is bounded above by e^ε . Note

that by (12), $p(\Theta = \mathcal{F}_{PPMTF}(\mathbf{R})) = p(\Theta|\mathbf{R}) > 0$ and $p(\Theta = \mathcal{F}_{PPMTF}(\mathbf{R}')) = p(\Theta|\mathbf{R}') > 0$. Then we obtain:

$$\begin{aligned}
& \frac{p(\Theta = \mathcal{F}_{PPMTF}(\mathbf{R}))}{p(\Theta = \mathcal{F}_{PPMTF}(\mathbf{R}'))} \\
&= \frac{\int_{\Theta} \exp[-G(\mathbf{R}, \Theta)] d\Theta}{\int_{\Theta} \exp[-G(\mathbf{R}', \Theta)] d\Theta} \quad (\text{by (12)}) \\
&= \frac{\exp[-G(\mathbf{R}, \Theta)]}{\exp[-G(\mathbf{R}', \Theta)]} \cdot \frac{\int_{\Theta} \exp[-G(\mathbf{R}', \Theta)] d\Theta}{\int_{\Theta} \exp[-G(\mathbf{R}, \Theta)] d\Theta} \\
&= \exp[-G(\mathbf{R}, \Theta) + G(\mathbf{R}', \Theta)] \cdot \frac{\int_{\Theta} \exp[-G(\mathbf{R}', \Theta)] d\Theta}{\int_{\Theta} \exp[-G(\mathbf{R}, \Theta)] d\Theta} \\
&\leq e^{\frac{\varepsilon}{2}} \cdot e^{\frac{\varepsilon}{2}} \cdot \frac{\int_{\Theta} \exp[-G(\mathbf{R}, \Theta)] d\Theta}{\int_{\Theta} \exp[-G(\mathbf{R}, \Theta)] d\Theta} \quad ((\text{by (13) and } \Delta G \leq \frac{\varepsilon}{2})) \\
&= e^{\varepsilon},
\end{aligned}$$

which proves Proposition 1. \square

D. DETAILS ON SGD

SGD [10] is a general synthetic generator for any kind of data, which works as follows: (i) Train the dependency structure (graph) between data attributes; (ii) Train conditional probabilities for each attribute given its parent attributes; (iii) Generate a synthetic data record from an input data record by copying the top $\gamma \in \mathbb{Z}_{\geq 0}$ attributes from the input data record and generating the remaining attributes using the trained conditional probabilities. Note that the dependency structure and the conditional probabilities are common to all users.

We applied **SGD** to synthesizing location traces as follows. We regarded an event as an attribute, and a location trace of length $|\mathcal{T}|$ as a data record with $|\mathcal{T}|$ attributes. Then it would be natural to consider that the dependency structure is given by the time-dependent Markov chain model as in **Proposal** and **SGLT**, and the conditional probabilities are given by the transition matrix for each time slot. In other words, we do not need to train the dependency structure; i.e., we can skip (i).

We trained the transition matrix for each time slot ($|\mathcal{L}| \times |\mathcal{X}| \times |\mathcal{X}|$ elements in total) and the visit-probability vector for the first time instant ($|\mathcal{X}|$ elements in total) from the training traces via maximum likelihood estimation. Then we synthesized a trace from an input training trace by copying the first γ events and generating the remaining events using the transition matrix (or the visit-probability vector for a location at the first time instant when $\gamma = 0$).

Note that we did not add the Laplacian noise to the transition matrices and the visit-probability vector (unlike [10]), since we assume that the parameters of the generative model are kept secret or discarded, as in [9] (see Section 2.2).

E. EFFECT OF SHARING FACTOR MATRICES

The proposed method (**Proposal**) shares the factor matrices **A** and **B** between two tensors. Here we show the effect of sharing **A** and **B**. Specifically, we compare the proposed method with a method that *independently* factorizes each tensor; i.e., factorizes \mathbf{R}^I into factor matrices $\mathbf{A}^I \in \mathbb{R}^{|\mathcal{U}| \times z}$, $\mathbf{B}^I \in \mathbb{R}^{|\mathcal{X}| \times z}$, $\mathbf{C}^I \in \mathbb{R}^{|\mathcal{X}| \times z}$, and \mathbf{R}^{II} into factor matrices $\mathbf{A}^{II} \in \mathbb{R}^{|\mathcal{U}| \times z}$, $\mathbf{B}^{II} \in \mathbb{R}^{|\mathcal{X}| \times z}$, $\mathbf{D}^{II} \in \mathbb{R}^{|\mathcal{L}| \times z}$. We train these

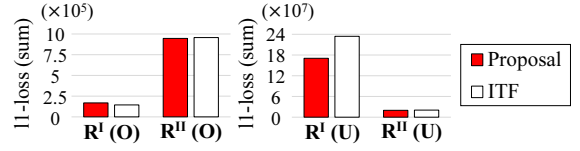


Figure 14: Reconstruction errors (sum of the l_1 loss) in \mathbf{R}^I and \mathbf{R}^{II} (TKY). “O” and “U” in the parentheses represent observed elements and unobserved elements, respectively.

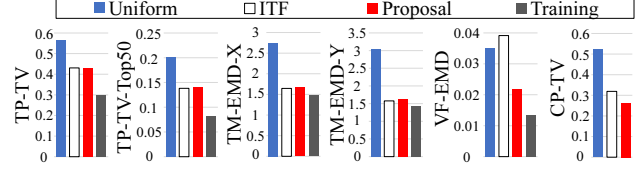


Figure 15: Utility of Proposal and ITF (TKY).

factor matrices via the Gibbs sampling, and then generate synthetic traces via the MH algorithm in the same way as **Proposal**. We denote this method by **ITF** (Independent Tensor Factorization).

We compare **Proposal** with **ITF** using the Foursquare dataset (**FS**). Here we selected Tokyo (**TKY**) as a city (we also evaluated the other cities and obtained similar results). We used the same parameters as in Section 4.2. Then we evaluated the reconstruction errors of \mathbf{R}^I and \mathbf{R}^{II} . Specifically, we evaluated the sum of the l_1 -loss (absolute error) between \mathbf{R}^I and $\hat{\mathbf{R}}^I$. We first evaluated the sum of the l_1 -loss for *observed elements* (i.e., positive elements or zero elements treated as 0s). Then we evaluated the sum of the l_1 -loss for *unobserved elements* (i.e., zero elements treated as missing). Note that the number of unobserved elements is very large. Specifically, let $\eta^I \in \mathbb{Z}_{\geq 0}$ be the total number of unobserved elements in \mathbf{R}^I . Then η^I is close to $|\mathcal{U}| \times |\mathcal{X}| \times |\mathcal{X}|$ ($= 47956 \times 1000 \times 1000$), as \mathbf{R}^I is very sparse (note that $\lambda^I = 10^2$ and $\rho^I = 10^3$, as described in Section 4.2). Thus, we randomly selected 1000 unobserved elements for each user and evaluated the sum of the l_1 -loss for the selected elements. Then we multiplied the l_1 -loss by $\frac{\eta^I}{1000|\mathcal{U}|}$ to estimate the l_1 -loss for all of the unobserved elements. We evaluated the l_1 -loss for the observed and unobserved elements in \mathbf{R}^{II} in the same way. We also evaluated all of the utility measures in Section 4.3.

Figure 14 shows the reconstruction errors in \mathbf{R}^I and \mathbf{R}^{II} . It can be seen that **Proposal** significantly outperforms **ITF** with regard to the reconstruction error of unobserved elements in \mathbf{R}^I . This is because \mathbf{R}^I (which contains $47956 \times 1000 \times 1000$ elements) is much more sparse than \mathbf{R}^{II} (which contains $47956 \times 1000 \times 24$ elements), and \mathbf{R}^{II} compensates for the sparseness of \mathbf{R}^I in **Proposal** by sharing **A** and **B**. This is consistent with the experimental results in [65], where multiple tensor factorization works well especially when one of two tensors is extremely sparse.

Figure 15 shows the utility of **Proposal** and **ITF** (here we do not run the PD test; even if we use the (10, 1)-PD test, the utility of **Proposal** is hardly changed, as shown in Section F). It can be seen that **Proposal** significantly outperforms **ITF** with regard to **VF-EMD** and **CP-TV**.

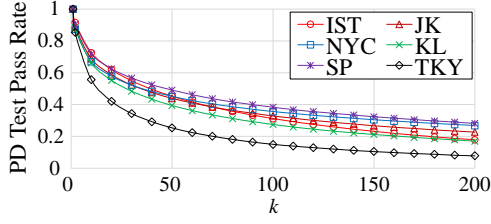


Figure 16: Relationship between k and the PD test pass rate.

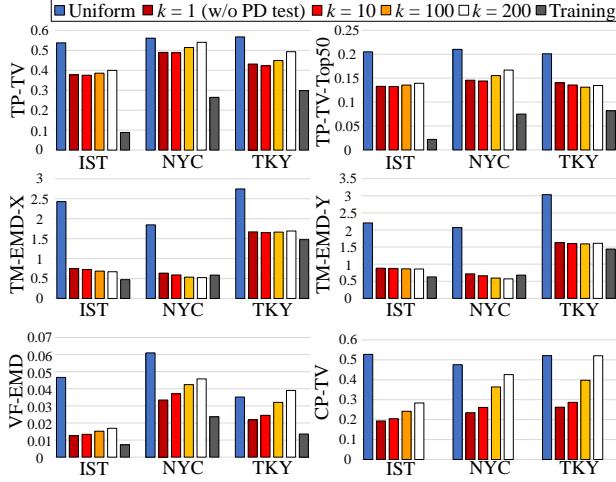


Figure 17: Utility of Proposal with $k = 1, 10, 100$, or 200 (IST, NYC, and TKY).

We consider this is because **Proposal** trains \mathbf{A} and \mathbf{B} , which model the similarity structure among users and locations, respectively, more accurately by sharing them between \mathbf{R}^I and \mathbf{R}^{II} . Consequently, **Proposal** generates user-specific (or cluster-specific) traces more effectively.

In summary, **Proposal** addresses the sparseness of \mathbf{R}^I and achieves high utility by sharing factor matrices.

F. EFFECT OF K IN THE PD TEST

Here we analyze the effect of k in (k, ε) -PD on the performance of the proposed method (**Proposal**). Specifically, we changed k from 1 to 200 in the experiments using the Foursquare dataset (**FS**). We set the other parameters to the same values as in Section 4 (e.g., $\varepsilon = 1$, $|\mathcal{U}^*| = 32000$).

First, we evaluated the *PD test pass rate*, which is the proportion of synthetic traces that has passed the PD test to all synthetic traces. Figure 16 shows the results for six cities. It can be seen that the PD test pass rate decreases as increase in k . For example, the PD test pass rate is about 60% to 70% when $k = 10$ (as in Section 4), whereas it is about 20% to 40% when $k = 100$.

Next, we set k to $k = 1, 10, 100$, or 200 , and evaluated all of the utility measures in Section 4.3. Figure 17 shows the results for **IST**, **NYC**, and **TKY** (we confirmed that the results of the other cities were similar to those of **NYC** and **TKY**). Note that when $k = 1$, all of the synthetic traces pass the PD test. In other words, **Proposal** with $k = 1$ is equivalent to **Proposal** without the PD test.

It can be seen that all of the utility measures are hardly affected by running the PD test with $k = 10$ in all of the cities. In **NYC** and **TKY**, **VF-EMD** and **CP-TV** are significantly increased by increasing k from 10 to 200. However, in **IST**, all of the utility measures are not affected much even when $k = 200$. Note that when $k = 200$, the PD test pass rate of **IST** (17.9%) is lower than that of **NYC** (26.9%), as shown in Figure 16. Nevertheless, **Proposal** significantly outperforms **Uniform** with regard to all of the utility measures in **IST**. This is because the number of users is very large in **IST** ($|\mathcal{U}| = 219793$). Thus, even if the PD test pass rate is low, a large amount of synthetic traces still pass the test and preserves the statistical features of all users or each cluster.

In summary, **Proposal** achieves high utility and high privacy for various types of geo-data analysis, especially when the amount of the original location data is very large.

G. DETAILS ON THE GIBBS SAMPLING

We explain how to sample the hyper-parameters Ψ and the MTF parameters Θ using the Gibbs sampling in detail.

In the t -th iteration, we sample $\Psi_A^{(t)}$, $\Psi_B^{(t)}$, $\Psi_C^{(t)}$, $\Psi_D^{(t)}$, $\mathbf{A}^{(t)}$, $\mathbf{B}^{(t)}$, $\mathbf{C}^{(t)}$, and $\mathbf{D}^{(t)}$ from the conditional distribution given the current values of the other variables. Specifically, based on the graphical model in Figure 4, we sample each variable as follows:

$$\Psi_A^{(t)} \sim p(\Psi_A | \mathbf{A}^{(t-1)}) \quad (14)$$

$$\Psi_B^{(t)} \sim p(\Psi_B | \mathbf{B}^{(t-1)}) \quad (15)$$

$$\Psi_C^{(t)} \sim p(\Psi_C | \mathbf{C}^{(t-1)}) \quad (16)$$

$$\Psi_D^{(t)} \sim p(\Psi_D | \mathbf{D}^{(t-1)}) \quad (17)$$

$$\mathbf{A}^{(t)} \sim p(\mathbf{A} | \mathbf{R}, \mathbf{B}^{(t-1)}, \mathbf{C}^{(t-1)}, \mathbf{D}^{(t-1)}, \Psi_A^{(t)}) \quad (18)$$

$$\mathbf{B}^{(t)} \sim p(\mathbf{B} | \mathbf{R}, \mathbf{A}^{(t)}, \mathbf{C}^{(t-1)}, \mathbf{D}^{(t-1)}, \Psi_B^{(t)}) \quad (19)$$

$$\mathbf{C}^{(t)} \sim p(\mathbf{C} | \mathbf{R}^I, \mathbf{A}^{(t)}, \mathbf{B}^{(t)}, \Psi_C^{(t)}) \quad (20)$$

$$\mathbf{D}^{(t)} \sim p(\mathbf{D} | \mathbf{R}^{II}, \mathbf{A}^{(t)}, \mathbf{B}^{(t)}, \Psi_D^{(t)}) \quad (21)$$

Below we explain how to compute the sampling distribution for the hyper-parameters and MTF parameters in detail.

Sampling of the hyper-parameters. We explain the computation of the right-hand side of (14) in the Gibbs sampling. We omit the computation of (15), (16), and (17), as they are computed in the same way as (14); i.e., (15), (16), and (17) can be computed by replacing \mathbf{A} in (14) with \mathbf{B} , \mathbf{C} , and \mathbf{D} , respectively. Below we omit the superscripts (t) and $(t-1)$.

$p(\Psi_A | \mathbf{A})$ in (14) can be computed by using the fact that the Normal-Wishart distribution is a conjugate prior of the multivariate normal distribution [11]. Specifically, following [57], we compute $p(\Psi_A | \mathbf{A})$ in (14) as follows:

$$\begin{aligned} p(\Psi_A | \mathbf{A}) &= \frac{p(\mathbf{A} | \Psi_A) p(\Psi_A)}{p(\mathbf{A})} \quad (\text{by Bayes' theorem}) \\ &= \mathcal{N}(\mu_A | \mu_0^*, (\beta_0^* \Lambda_A)^{-1}) \mathcal{W}(\Lambda_A | W_0^*, \nu_0^*), \end{aligned} \quad (22)$$

where

$$\mu_0^* = \frac{\beta_0 \mu_0 + |\mathcal{U}| \bar{\mathbf{a}}}{\beta_0 + |\mathcal{U}|} \quad (23)$$

$$\beta_0^* = \beta_0 + |\mathcal{U}| \quad (24)$$

$$W_0^* = \left[W_0^{-1} + |\mathcal{U}| \bar{\mathbf{S}} + \frac{\beta_0 |\mathcal{U}|}{\beta_0 + |\mathcal{U}|} (\mu_0 - \bar{\mathbf{a}})^\top (\mu_0 - \bar{\mathbf{a}}) \right]^{-1} \quad (25)$$

$$\nu_0^* = \nu_0 + |\mathcal{U}| \quad (26)$$

$$\bar{\mathbf{a}} = \frac{1}{|\mathcal{U}|} \sum_{n=1}^{|\mathcal{U}|} \mathbf{a}_n \quad (27)$$

$$\bar{\mathbf{S}} = \frac{1}{|\mathcal{U}|} \sum_{n=1}^{|\mathcal{U}|} \mathbf{a}_n^\top \mathbf{a}_n. \quad (28)$$

Thus we compute $p(\Psi_{\mathbf{A}}|\mathbf{A})$ by (22) to (28), and then sample $\Psi_{\mathbf{A}}$ from $p(\Psi_{\mathbf{A}}|\mathbf{A})$.

Sampling of the MTF parameters. Next we explain the computation of (18) and (20). We omit the computation of (19) and (21), as they are computed in the same way as (18) and (20), respectively; i.e., (19) and (21) can be computed by exchanging \mathbf{A} for \mathbf{B} in (19), and \mathbf{C} for \mathbf{D} in (21).

$p(\mathbf{A}|\mathbf{R}, \mathbf{B}, \mathbf{C}, \mathbf{D}, \Psi_{\mathbf{A}})$ in (18) can be written as follows:

$$p(\mathbf{A}|\mathbf{R}, \mathbf{B}, \mathbf{C}, \mathbf{D}, \Psi_{\mathbf{A}}) = \prod_{n=1}^{|\mathcal{U}|} p(\mathbf{a}_n|\mathbf{R}_n^{\mathbf{I}}, \mathbf{R}_n^{\mathbf{II}}, \mathbf{B}, \mathbf{C}, \mathbf{D}, \Psi_{\mathbf{A}}), \quad (29)$$

where $\mathbf{R}_n^{\mathbf{I}}$ and $\mathbf{R}_n^{\mathbf{II}}$ are the n -th matrices in $\mathbf{R}^{\mathbf{I}}$ and $\mathbf{R}^{\mathbf{II}}$, respectively. By Bayes' theorem and the graphical model in Figure 4, $p(\mathbf{a}_n|\mathbf{R}_n^{\mathbf{I}}, \mathbf{R}_n^{\mathbf{II}}, \mathbf{B}, \mathbf{C}, \mathbf{D}, \Psi_{\mathbf{A}})$ in (29) can be written as follows:

$$\begin{aligned} & p(\mathbf{a}_n|\mathbf{R}_n^{\mathbf{I}}, \mathbf{R}_n^{\mathbf{II}}, \mathbf{B}, \mathbf{C}, \mathbf{D}, \Psi_{\mathbf{A}}) \\ &= \frac{p(\mathbf{R}_n^{\mathbf{I}}, \mathbf{R}_n^{\mathbf{II}}|\mathbf{a}_n, \mathbf{B}, \mathbf{C}, \mathbf{D}, \Psi_{\mathbf{A}})p(\mathbf{a}_n|\mathbf{B}, \mathbf{C}, \mathbf{D}, \Psi_{\mathbf{A}})}{p(\mathbf{R}_n^{\mathbf{I}}, \mathbf{R}_n^{\mathbf{II}}|\mathbf{B}, \mathbf{C}, \mathbf{D}, \Psi_{\mathbf{A}})} \\ &= \frac{p(\mathbf{R}_n^{\mathbf{I}}|\mathbf{a}_n, \mathbf{B}, \mathbf{C})p(\mathbf{R}_n^{\mathbf{II}}|\mathbf{a}_n, \mathbf{B}, \mathbf{D})p(\mathbf{a}_n|\Psi_{\mathbf{A}})}{p(\mathbf{R}_n^{\mathbf{I}}, \mathbf{R}_n^{\mathbf{II}}|\mathbf{B}, \mathbf{C}, \mathbf{D}, \Psi_{\mathbf{A}})}. \end{aligned} \quad (30)$$

Note that $p(\mathbf{R}_n^{\mathbf{I}}|\mathbf{a}_n, \mathbf{B}, \mathbf{C})$, $p(\mathbf{R}_n^{\mathbf{II}}|\mathbf{a}_n, \mathbf{B}, \mathbf{D})$, and $p(\mathbf{a}_n|\Psi_{\mathbf{A}})$ are normal distributions (as described in Section 3.3), and $p(\mathbf{R}_n^{\mathbf{I}}, \mathbf{R}_n^{\mathbf{II}}|\mathbf{B}, \mathbf{C}, \mathbf{D}, \Psi_{\mathbf{A}})$ is a normalization constant so that the sum of $p(\mathbf{a}_n|\mathbf{R}_n^{\mathbf{I}}, \mathbf{R}_n^{\mathbf{II}}, \mathbf{B}, \mathbf{C}, \mathbf{D}, \Psi_{\mathbf{A}})$ over all values of \mathbf{a}_n is one. In addition, by (3), $\hat{r}_{n,i,j}^{\mathbf{I}}$ and $\hat{r}_{n,i,j}^{\mathbf{II}}$ can be expressed as: $\hat{r}_{n,i,j}^{\mathbf{I}} = \mathbf{a}_n^\top \mathbf{b}_{c_{ij}}$ and $\hat{r}_{n,i,j}^{\mathbf{II}} = \mathbf{a}_n^\top \mathbf{b}_{d_{ij}}$, respectively, where \circ represents the Hadamard product.

Thus, $p(\mathbf{a}_n|\mathbf{R}_n^{\mathbf{I}}, \mathbf{R}_n^{\mathbf{II}}, \mathbf{B}, \mathbf{C}, \mathbf{D}, \Psi_{\mathbf{A}})$ can be expressed as:

$$\begin{aligned} & p(\mathbf{a}_n|\mathbf{R}_n^{\mathbf{I}}, \mathbf{R}_n^{\mathbf{II}}, \mathbf{B}, \mathbf{C}, \mathbf{D}, \Psi_{\mathbf{A}}) \\ &= d_1 \exp \left[\sum_{i=1}^{|\mathcal{X}|} \sum_{j=1}^{|\mathcal{X}|} \alpha I_{n,i,j}^{\mathbf{I}} (\mathbf{a}_n^\top \mathbf{b}_{c_{ij}} - r_{n,i,j}^{\mathbf{I}})^2 \right. \\ & \quad \left. + \sum_{i=1}^{|\mathcal{X}|} \sum_{j=1}^{|\mathcal{L}|} \alpha I_{n,i,j}^{\mathbf{II}} (\mathbf{a}_n^\top \mathbf{b}_{d_{ij}} - r_{n,i,j}^{\mathbf{II}})^2 \right. \\ & \quad \left. + (\mathbf{a}_n - \mu_{\mathbf{A}})^\top \Lambda_{\mathbf{A}} (\mathbf{a}_n - \mu_{\mathbf{A}}) \right], \end{aligned} \quad (31)$$

where $d_1 \in \mathbb{R}$ is a normalization constant, and $\mathbf{b}_{c_{ij}} \in \mathbb{R}^z$ and $\mathbf{b}_{d_{ij}} \in \mathbb{R}^z$ are shorthand for $\mathbf{b}_i \circ \mathbf{c}_j$ and $\mathbf{b}_i \circ \mathbf{d}_j$, respectively.

To simplify (29) and (31), we use the following two facts. First, for any $v \in \mathbb{R}$ and any $\mathbf{w} \in \mathbb{R}^z$, we obtain:

$$\begin{aligned} v^2 &= v(\mathbf{w}^{-1\top} \mathbf{w})(\mathbf{w}^\top \mathbf{w}^{-1})v \\ &= ((v\mathbf{w}^{-1})^\top \mathbf{w})(\mathbf{w}^\top (v\mathbf{w}^{-1})) \\ &= (v\mathbf{w}^{-1})^\top (\mathbf{w}\mathbf{w}^\top) (v\mathbf{w}^{-1}) \quad (\text{by associative property}). \end{aligned}$$

Thus,

$$\begin{aligned} & (\mathbf{a}_n^\top \mathbf{b}_{c_{ij}} - r_{n,i,j}^{\mathbf{I}})^2 \\ &= (\mathbf{a}_n - r_{n,i,j}^{\mathbf{I}} \mathbf{b}_{c_{ij}}^{-1})^\top (\mathbf{b}_{c_{ij}} \mathbf{b}_{c_{ij}}^\top) (\mathbf{a}_n - r_{n,i,j}^{\mathbf{I}} \mathbf{b}_{c_{ij}}^{-1}) \\ & (\mathbf{a}_n^\top \mathbf{b}_{d_{ij}} - r_{n,i,j}^{\mathbf{II}})^2 \\ &= (\mathbf{a}_n - r_{n,i,j}^{\mathbf{II}} \mathbf{b}_{d_{ij}}^{-1})^\top (\mathbf{b}_{d_{ij}} \mathbf{b}_{d_{ij}}^\top) (\mathbf{a}_n - r_{n,i,j}^{\mathbf{II}} \mathbf{b}_{d_{ij}}^{-1}), \end{aligned}$$

and hence

$$\begin{aligned} & p(\mathbf{a}_n|\mathbf{R}_n^{\mathbf{I}}, \mathbf{R}_n^{\mathbf{II}}, \mathbf{B}, \mathbf{C}, \mathbf{D}, \Psi_{\mathbf{A}}) \\ &= d_2 \prod_{i=1}^{|\mathcal{X}|} \prod_{j=1}^{|\mathcal{X}|} \mathcal{N}(\mathbf{a}_n | r_{n,i,j}^{\mathbf{I}} \mathbf{b}_{c_{ij}}^{-1}, \alpha I_{n,i,j}^{\mathbf{I}} (\mathbf{b}_{c_{ij}} \mathbf{b}_{c_{ij}}^\top)^{-1}) \\ & \quad \cdot \prod_{i=1}^{|\mathcal{X}|} \prod_{j=1}^{|\mathcal{L}|} \mathcal{N}(\mathbf{a}_n | r_{n,i,j}^{\mathbf{II}} \mathbf{b}_{d_{ij}}^{-1}, \alpha I_{n,i,j}^{\mathbf{II}} (\mathbf{b}_{d_{ij}} \mathbf{b}_{d_{ij}}^\top)^{-1}) \\ & \quad \cdot \mathcal{N}(\mathbf{a}_n | \mu_{\mathbf{A}}, \Lambda_{\mathbf{A}}^{-1}), \end{aligned} \quad (32)$$

where $d_2 \in \mathbb{R}$ is a normalization constant.

Second, the product of two Gaussian densities is proportional to a Gaussian density [52]. Specifically, for any $\mathbf{w} \in \mathbb{R}^z$, any $\mathbf{m}_1, \mathbf{m}_2 \in \mathbb{R}^z$, and any $\Lambda_1, \Lambda_2 \in \mathbb{R}^{z \times z}$, we obtain:

$$\mathcal{N}(\mathbf{w}|\mathbf{m}_1, \Lambda_1^{-1}) \cdot \mathcal{N}(\mathbf{w}|\mathbf{m}_2, \Lambda_2^{-1}) = d_3 \mathcal{N}(\mathbf{w}|\mathbf{m}_c, \Lambda_c^{-1}), \quad (33)$$

where

$$\begin{aligned} d_3 &= \mathcal{N}(\mathbf{m}_1|\mathbf{m}_2, \Lambda_1^{-1} + \Lambda_2^{-1}) \\ \mathbf{m}_c &= (\Lambda_1 + \Lambda_2)^{-1} (\Lambda_1 \mathbf{m}_2 + \Lambda_2 \mathbf{m}_1) \\ \Lambda_c &= \Lambda_1 + \Lambda_2. \end{aligned} \quad (34)$$

By (32), (33), and (34), $p(\mathbf{A}|\mathbf{R}, \mathbf{B}, \mathbf{C}, \mathbf{D}, \Psi_{\mathbf{A}})$ in (29) can be written as follows:

$$p(\mathbf{A}|\mathbf{R}, \mathbf{B}, \mathbf{C}, \mathbf{D}, \Psi_{\mathbf{A}}) = \prod_{n=1}^{|\mathcal{U}|} \mathcal{N}(\mathbf{a}_n | \mu_{\mathbf{A},n}^*, \Lambda_{\mathbf{A},n}^*), \quad (35)$$

where

$$\begin{aligned} \Lambda_{\mathbf{A},n}^* &= \Lambda_{\mathbf{A}} + \alpha I_{n,i,j}^{\mathbf{I}} \sum_{i=1}^{|\mathcal{X}|} \sum_{j=1}^{|\mathcal{X}|} (\mathbf{b}_{c_{ij}} \mathbf{b}_{c_{ij}}^\top) \\ & \quad + \alpha I_{n,i,j}^{\mathbf{II}} \sum_{i=1}^{|\mathcal{X}|} \sum_{j=1}^{|\mathcal{L}|} (\mathbf{b}_{d_{ij}} \mathbf{b}_{d_{ij}}^\top) \\ \mu_{\mathbf{A},n}^* &= [\Lambda_{\mathbf{A},n}^*]^{-1} \left(\Lambda_{\mathbf{A}} \mu_{\mathbf{A}} + \alpha I_{n,i,j}^{\mathbf{I}} \sum_{i=1}^{|\mathcal{X}|} \sum_{j=1}^{|\mathcal{X}|} r_{n,i,j}^{\mathbf{I}} \mathbf{b}_{c_{ij}} \right. \\ & \quad \left. + \alpha I_{n,i,j}^{\mathbf{II}} \sum_{i=1}^{|\mathcal{X}|} \sum_{j=1}^{|\mathcal{L}|} r_{n,i,j}^{\mathbf{II}} \mathbf{b}_{d_{ij}} \right). \end{aligned} \quad (36)$$

Similarly, $p(\mathbf{C}|\mathbf{R}^{\mathbf{I}}, \mathbf{A}, \mathbf{B}, \Psi_{\mathbf{C}})$ in (20) can be written as follows:

$$\begin{aligned} p(\mathbf{C}|\mathbf{R}^{\mathbf{I}}, \mathbf{A}, \mathbf{B}, \Psi_{\mathbf{C}}) &= \prod_{j=1}^{|\mathcal{X}|} p(\mathbf{c}_j|\mathbf{R}^{\mathbf{I}}, \mathbf{A}, \mathbf{B}, \Psi_{\mathbf{C}}) \\ &= \prod_{j=1}^{|\mathcal{X}|} \mathcal{N}(\mathbf{c}_j | \mu_{\mathbf{C},j}^*, \Lambda_{\mathbf{C},j}^*), \end{aligned} \quad (38)$$

where

$$\Lambda_{\mathbf{C},j}^* = \Lambda_{\mathbf{C}} + \alpha I_{n,i,j}^{\mathbf{I}} \sum_{n=1}^{|\mathcal{U}|} \sum_{i=1}^{|\mathcal{X}|} \mathbf{a}\mathbf{b}_{ni} \mathbf{a}\mathbf{b}_{ni}^{\top} \quad (39)$$

$$\mu_{\mathbf{C},j}^* = [\Lambda_{\mathbf{C},j}^*]^{-1} \left(\Lambda_{\mathbf{C}} \mu_{\mathbf{C}} + \alpha I_{n,i,j}^{\mathbf{I}} \sum_{n=1}^{|\mathcal{U}|} \sum_{i=1}^{|\mathcal{X}|} r_{n,i,j}^{\mathbf{I}} \mathbf{a}\mathbf{b}_{ni} \right) \quad (40)$$

and $\mathbf{a}\mathbf{b}_{ni}$ is shorthand for $\mathbf{a}_n \circ \mathbf{b}_i$. Thus we compute $p(\mathbf{A}|\mathbf{R}, \mathbf{B}, \mathbf{C}, \mathbf{D}, \Psi_{\mathbf{A}})$ and $p(\mathbf{C}|\mathbf{R}^{\mathbf{I}}, \mathbf{A}, \mathbf{B}, \Psi_{\mathbf{C}})$ by (35) to (37) and (38) to (40), respectively. Then we sample \mathbf{A} and \mathbf{C} from these distributions.